UNIVERSIDADE DA BEIRA INTERIOR

Engenharia

Cam design and implementation to a single-cylinder engine to allow for high-altitude operation

(Versão revista após discussão)

Francisco Ferreira dos Santos Corrêa Figueira

Dissertação para obtenção do Grau de Mestre em

Engenharia Aeronáutica

(Ciclo de estudos integrado)

Orientador: Prof. Doutor Francisco Miguel Ribeiro Proença Brójo

Covilhã, julho de 2019

Acknowledgements

I would like to thank everybody who had any implication whatsoever in this project, for without each and every one of them, it would not have been possible, for me, to finish this work.

Firstly, I would like to thank my supervisor, Professor Francisco Miguel Ribeiro Proença Brójo, for all the knowledge, patience, help and guidance shown throughout the development of this dissertation. It would not have been possible without his motivation and constant optimism.

Secondly, to the DCA's technician and operational assistant, Mr Rui Manuel Tomé Paulo, who had to put up with my constant requests for tools and other materials, always with a smile on his face and still managing to help with the experiment, in the process. When it came to the experimental procedure, I would like to thank Alexandre Nunes for the support, João Rocha for the constant help and great tips, Leonardo Batista and Miguel Calmeiro for the endless days and nights spent at the hangar trying to successfully complete the test runs. Also, to Mara Andrade for putting up with my constant bad mood and still supporting me every day through this journey, to Fábio Morais for the constant support and help through these hard months, and finally to Ana Margarida, Catarina Lopes, David Quintino, Filipe Vinhas, João Prates, and Pedro Dias for all the years they have stayed by my side.

Furthermore, I would like to thank my friends who, throughout the years, formed a second family for me, away from home. Thank you to André Franco, António Lopes, Cátia Miguel, Cátia Moura, Daniel Rodrigues, Daniela Matos, Fabiana Contessoto, Flávia Morais, Gabriel Carrolo, Hélder Gonçalves, Inês Ferrão, Ivo Fernandes, João Morgado, Lídia Lobo, Luís Fialho, Luís Santos, Nídia, Rodolfo Lopes, Rute Neves and all the members of both TEATRUBI and the UBI tennis team.

And last, but certainly not least, to my parents, brother, sisters and every single member of my family for the unconditional support throughout the years, you make me believe that family really does come first, and this journey was certainly made easier due to your presence.

Resumo

O design de cames é uma área extremamente complexa e vasta, devido ao facto de ter uma gama de aplicações muito versátil, possível de adaptar para uma grande variedade de sistemas mecânicos. Quando este tipo de estudo é aplicado a motores a pistão, com sistemas de válvulas intrínsecos aos mesmos, podem obter-se resultados muito positivos, ou negativos, tal como fazem os grandes fabricantes da indústria automóvel, que tentam, através da implementação deste tipo de estudos nos seus motores, melhorar o seu desempenho e consumo de combustível. Contudo, no que toca a possíveis sistemas propulsivos para aeronaves não tripuladas (ou UAVs), não existem muitos estudos já feitos acerca deste assunto, devido às condições adversas que estes tipos de motores enfrentam aquando de altitudes elevadas.

O presente trabalho foi feito com o intuito de verificar se é, ou não, possível, adaptar um motor monocilíndrico para funcionar com uma hélice e como meio de propulsão de um pequeno UAV em desenvolvimento pela Universidade da Beira Interior (ou UBI), através da alteração do sistema came-seguidor. O motor selecionado para este projeto, o Honda GX31, é um motor extremamente rotativo e, por isso, o objetivo principal será aumentar o alcance da gama de rotações do motor e mover os picos de binário e potência para regimes de rotação mais baixos, sem sacrificar em demasia esses valores. De forma a atingir esse fim, será necessário alterar o *timing* das válvulas do motor, através da alteração do próprio perfil da came, devido a este motor ter um sistema came-seguidor muito peculiar, em que apenas uma came controla ambas as válvulas.

No final deste documento são apresentados e discutidos os resultados obtidos experimentalmente, e que levam à conclusão de que é possível ter um grande sucesso nesta área, seguindo os procedimentos relatados nesta dissertação, dado que foi possível aumentar a gama de rotações do motor e reduzir os picos de binário e potência, sem comprometer demasiado os seus valores.

Palavras-chave

Árvore de cames, came, seguidor, motor de combustão interna, design de cames, mecanismo,

Abstract

Cam design is a very complex and vast study, due to the fact that its' applications are very versatile and can be adapted to work with many different mechanical systems. When applied to piston engines comprised of valve trains, this type of study can have a very positive, or negative, impact on the engine's performance output, like with popular car manufacturers that implement these studies into their engines, in order to enhance their performance and fuel consumption. When dealing with possible Unmanned Aerial Vehicles (or UAVs) propulsion systems, however, not many studies have been done in the past, due to the harsh conditions the engines have to endure at higher altitudes.

The present work tries to assess the possibility of altering the cam-follower system of a single-cylinder engine, in order to adapt it and allow it to work with a propeller, to use as a propulsion system for a UAV in development by Universidade da Beira Interior (or UBI). Due to the fact that the selected engine, the Honda GX31, is a very high-revving engine, the main target would be to broaden the usable power band of the engine and move the maximum torque and power values to lower engine speeds, without compromising those values too much. This should be achieved by altering the valve timing, through alteration of the cam profile itself, since for this particular engine, only one cam lobe controls both the intake and exhaust valves.

At the end of this document, the full experimental results are displayed and discussed, leading to the conclusion that it is possible to have success by following the path this dissertation has carved, since the usable power band was broadened and the reduction in terms of performance output was minimal.

Keywords

Camshaft, cam, follower, internal combustion engine, valve timing, cam design, mechanism

Table of Contents

List of Figures

List of Tables

Nomenclature

a	Acceleration	[mm/(°)^2]
C_n	Constant Coefficients	[-]
g	Gravitational Acceleration Constant	[m/s^2]
$\dot{f}$	Fuel Flow	[g/s]
j	Jerk	[mm/(°)^3]
L	Valve Lift	[mm]
$L_{1/4}$	Valve Lift at ¼ of the duration	[mm]
P	Power	[W]
R_1	Length	[mm]
R_2	Length	[mm]
R_3	Length	[mm]
R_4	Length	[mm]
R_b	Cam Base Circle Radius	[mm]
R_{cam}	Cam Radius (variable)	[mm]
s	Follower Displacement	[mm]
SFC	Specific Fuel Consumption	[g/kW.h]
T	Torque	[N.m]
v	Velocity	[mm/°]

Greek Symbols

α	Variable Angle	[º]
β	Valve duration	[º]
δ_1	Variable Angle	[º]
δ_2	Variable Angle	[º]
δ_3	Variable Angle	[º]
δ_4	Fixed Angle	[º]
θ	Crankshaft Rotation Angle	[º]
σ	Contact Stress	[Pa]
σ_{max}	Maximum Contact Stress	[Pa]
φ	Fixed Angle	[º]

List of Acronyms

aBDC	After Bottom Dead Center
aTDC	After Top Dead Center
bBDC	Before Bottom Dead Center
bTDC	Before Top Dead Center
BC	Boundary Condition
BEC	Battery Eliminator Circuit
cA	Camshaft Rotation Angle
CA	Crankshaft Rotation Angle
CI	Compression Ignition
DOHC	Double Overhead Camshaft
DCA	Department of Aerospace Sciences
DEM	Department of Electromechanical Engineering
DT	Dout
EEVC	Early Exhaust Valve Closing
EEVO	Early Exhaust Valve Opening
EIVC	Early Intake Valve Closing
EIVO	Early Intake Valve Opening
EVO	Exhaust Valve Opening
EVC	Exhaust Valve Closing
GND	Ground
IVO	Intake Valve Opening
IVC	Intake Valve Closing
SFC	Specific Fuel Consumption
SI	Spark Ignition
SOHC	Single Overhead Camshaft
TDC	Top Dead Center
UAV	Unmanned Aerial Vehicle
UBI	Universidade da Beira Interior
VTEC	Variable Valve Timing & Lift Electronic Control
WOT	Wide Open Throttle

Chapter 1

Introduction

1.1 Motivation

In a time where Unmanned Aerial Vehicles (or UAVs) are becoming very popular throughout most sectors of our society, the improvement of propulsion systems that can be used in UAVs is becoming more and more vital. Technology development when it comes to UAV propulsion systems is of vital importance, not only when it comes to jet engines and gas turbines, but also when it comes to regular piston engines that have to be optimized for aerial environments.

Despite the fact that internal combustion engines, or ICEs, have been vastly studied and developed throughout the years since their invention when it comes to improving the performance behaviour of a specific system within the engine, many challenges and obstacles are often found. With the knowledge that UAVs can be used in a wide variety of applications and sectors, finding the adequate propulsion system for any specific case becomes crucial for the further development of these aerial means of transportation.

Having the privilege of studying at Universidade da Beira Interior, or UBI, means that students can get involved in the many projects developed within, and from there comes the main drive of making this dissertation, which aims to verify if single-cylinder engines, like the Honda GX31 and GX35, can be improved, specifically through the alteration of the cam-follower system, to function as a propulsion system for a UAV, to be developed by the Department of Aerospace Sciences, or DCA, within UBI. Many engine manufacturers have developed, throughout the years, systems that enable the variation of the cam-follower systems and drivetrains, in order to improve the engine's performance, when applied to the automotive industry, however, when it comes to the aeronautical industry, this course of action has not been much pursued, due to the fact that most of the mentioned systems require high engine speeds in order to function efficiently, and with most multi-cylinder, piston engine powered lightweight aircraft, this condition is not met. On the other hand, when it comes to small UAVs, small engines with greater engine speeds can be implemented, with different valve train and cam-follower system configurations, meaning that it is important to, at least, try to verify the viability of using these as propulsion systems.

1.2 Objectives

The main purpose of the present dissertation is to assess the possibility of broadening the usable power band of a single cylinder piston engine, the Honda GX31, by altering its' cam-follower system, in order to fit the engine with a viable propeller and use it as a propulsion system for a UAV that is to be developed by UBI. In order to meet this objective, the following tasks were proposed:

- Analyse the original cam-follower system, with emphasis on the timing of the valve train and the cam-follower system motion;
- Design a new cam profile to meet the desired requirements without largely compromising the engine's performance;
- Manufacture and implement the new cam to the engine and experimentally compare the performance outputs and usable power bands of both the original and new cam configurations.

1.3 Dissertation outline

This dissertation is divided into 5 chapters, with the first and current one including the motivation and objectives.

The second chapter is dedicated to the literature review, in which the operating basics of the piston engine are presented, as well as an in-depth description of the different components of the valve train, their applications and the effect of changing the duration and lift of the valves and the shape of the cam profile. Moreover, an analysis of the complex study of cam design is presented, reasons are given to justify the choice of a specific motion function, with different examples of both more basic functions and very versatile ones.

An analysis of the Honda GX31 cam-follower system is made in the third chapter, in order to endorse the possibility of dimensioning the original cam profile and creating a new one to meet the expected requirements. This chapter is divided into four sub-sections, with the first one describing the procedure that was followed in order to measure the original cam's valve lift and an analysis of the resulting data, the second one detailing the mathematical method used to derive the needed equations and plot the data, the third one shows the Honda GX31 cam-follower system analysis, detailing the procedure that was followed in order to get the Cartesian coordinates of the original cam profile and finally, the last sub-section was written to elucidate the design of the new cam profile and a brief structural analysis to make sure there is no risk of damaging the engine components upon installation of the new part.

In the fourth chapter, the experimental components and test run procedures are detailed, as well as the experimental results, discussion and adversities encountered.

Lastly, the fifth chapter includes the dissertations' conclusions and possibilities for future work on this subject.

Chapter 2

Literature review

2.1 Piston engine operating basics

Although there is a very wide variety of piston engine types, we will only focus on reciprocating engines or, in other words, engines in which the piston moves back and forth inside the cylinder, transmitting the power through a connecting rod and crankshaft mechanism to the drive shaft [1] as represented in Figure 2.1. There are also other parameters represented which are important for the comprehension of the piston engine working mechanism, such as:

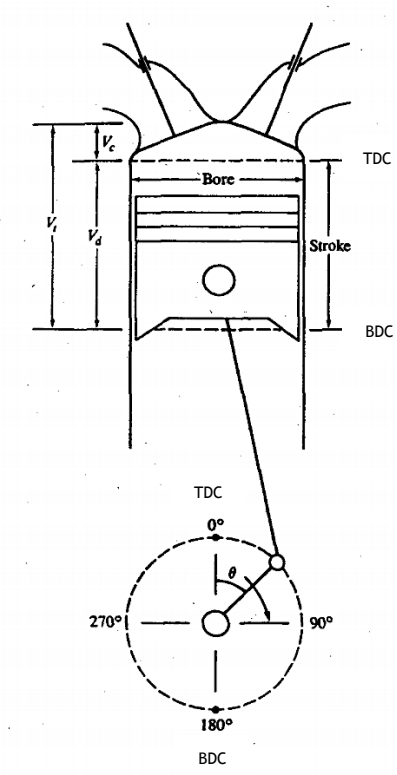

Figure 2.1 – Adapted cylinder movement schematics for a four-stroke engine [1]

Top-Dead-Centre (TDC), Bottom-Dead-Centre (BDC), bore, stroke, θ represents the crankshaft rotation angle, or CA (in degrees), V_d represents the volume that is displaced inside the cylinder, V_c represents the volume inside the combustion chamber and V_t represents the total volume of the cylinder. The ratio between the maximum and minimum volumes is called the compression ratio,

which has typical values of 8 to 12 for spark ignition, or SI engines and 12 to 24 for compression ignition, or CI engines [1].

In order to better understand the working mechanism of the engine, there are other important components worth mentioning, as we can see in Figure 2.2, which is an example of an SI, four-stroke[1] piston engine cut view.

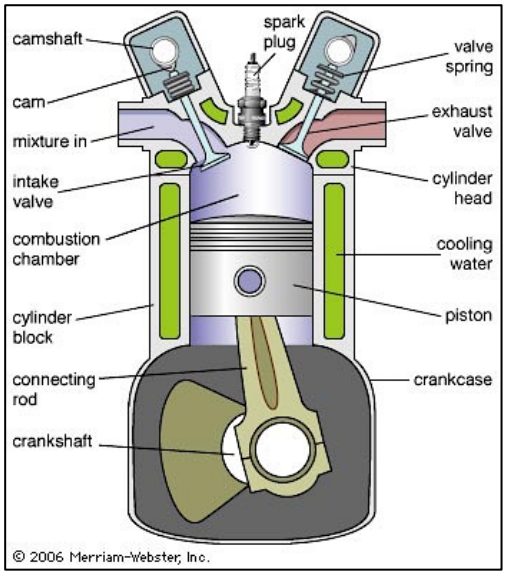

Figure 2.2 - Cylinder configuration of an SI, four-stroke, DOHC piston engine [2]

The components shown in Figure 2.2 are briefly described as follows:

- **Camshaft and Cam** - responsible for the opening and closing of the valves and will be discussed in depth later in the document;
- **Intake Valve** – lets in the air, fuel or mixture, depending on the configuration;
- **Exhaust Valve** – lets the burned mixture out of the cylinder;
- **Valve Spring** – if configured accurately, helps the valves close at the desired timing;
- **Spark Plug**[2] - responsible for emitting a spark in order to ignite the air/fuel mixture inside the cylinder;
- **Combustion Chamber** – the portion of the cylinder in which the combustion of the mixture happens;
- **Connecting rod** – connects the piston to the crankshaft;
- **Crankshaft** – connected to both the driveshaft and the connecting rod, it rotates twice per cycle in order to move the piston up and down;

[1] Four-stroke engine is one of the classifications given to piston engines, which will be featured in section 2.2.2.

[2] Only appears in SI engines, differing from the CI piston engines.

- **Piston** – connected to the crankshaft by a connecting rod, it moves up and down in order to transmit the forces derived from the combustion and pressure inside the cylinder to the crankshaft.

In order to accurately understand the working mechanism of a piston engine, however, we must also introduce the basic thermodynamic concepts behind it. An ICE's basic principle is to transform the thermal energy, obtained through the chemical reactions of the fuel and air mixture, into mechanical energy, a transformation which occurs according to a thermodynamic cycle. Most ICEs work according to the Otto cycle (which will be described in section 2.2 of this document), but there are other cycles which are worth mentioning like the Diesel cycle, the Miller cycle and the Atkinson cycle.

2.2 Piston engine classification

2.2.1 According to the thermodynamic cycle

2.2.1.1 Otto cycle

One of the most common and known ICE thermodynamic cycles is the Otto cycle, so named after Nikolaus August Otto, who discovered it in 1897 [3]. It is still widely used nowadays when it comes to piston engines, and it's working process is as follows:

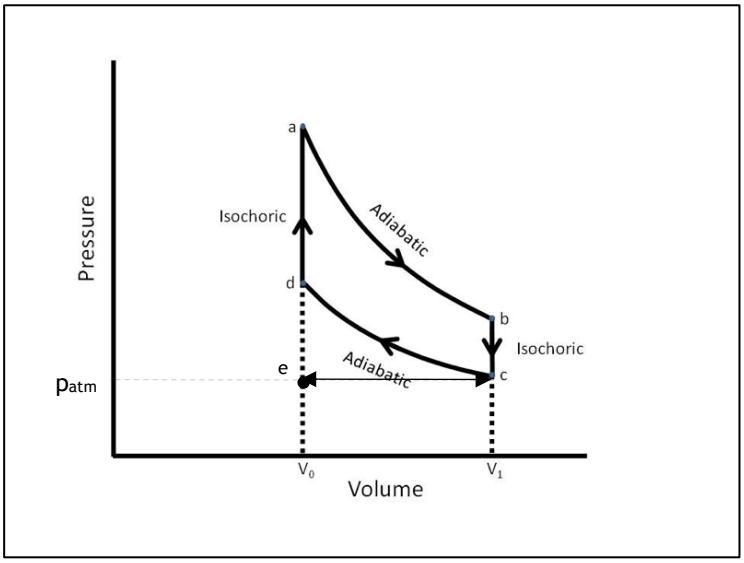

Figure 2.3 - Adapted Theoretical Otto Cycle Diagram (p,V) [4]

In the diagram shown above, we have the following stages:

- **e-c**: Isobaric intake (there are no pressure changes while the air enters the intake manifold and, afterwards, the cylinder);
- **c-d**: Adiabatic/Isentropic compression (there are no heat exchanges with the outside as the volume decreases and the piston travels up inside the cylinder creating a compression);
- **d-a**: Isochoric combustion (there are no volume changes as the pressure increases and the combustion occurs);
- **a-b**: Adiabatic/Isentropic expansion of the power stroke (there are no heat exchanges with the outside as the volume increases and the pressure decreases, due to the piston's downwards movement);
- **b-c**: Isochoric expansion (the exhaust valve opens, there are no volume changes as the burnt gases exit the cylinder and the pressure decreases);
- **c-e**: Isobaric exhaust (there are no pressure changes while the air leaves the exhaust manifold).

In Figure 2.3 is described, of course, a theoretical model of the ideal Otto cycle, and doesn't take into account a lot of variables, such as: both the intake and exhaust phases not being completely isobaric; the combustion not being instantaneous and isochoric; the compression, first and second expansion phases not being adiabatic/isentropic; the third expansion phase not being instantaneous and isochoric and the opening and closing of both the intake and exhaust valves not being instantaneous. Having said this, it's important to know the differences between the actual Otto cycle representation and the ideal (theoretical) one, as shown in Figure 2.4.

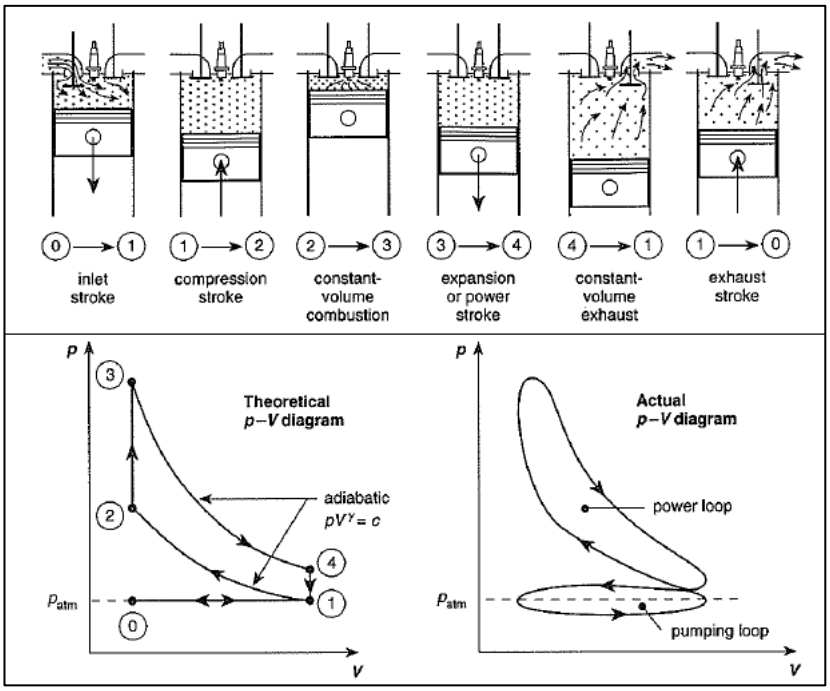

Figure 2.4 - Theoretical Otto Cycle diagram VS Actual Otto Cycle diagram [5]

Even though there are other thermodynamic cycles still used nowadays, they will not be further discussed in this particular document.

2.2.2 According to the work cycle

Piston engines, as a general rule, can be divided into two main categories, when it comes to work cycle[3]: two-stroke and four-stroke engines, and even though their final objective is the same, they have different working mechanisms and performance results (weight, power output, SFC, etc.). In this section, we will analyse the differences between these two engine categories.

2.2.2.1 Four-Stroke Engines

The vast majority of reciprocating engines operate according to the four-stroke work cycle which means, as the name would suggest, that each cylinder of the engine requires four strokes of its piston (this can also be translated to two crankshaft revolutions) to complete what is known as a full power stroke. This cycle works for both SI and CI engines, and contains the following phases [1] (see Fig. 2.5):

1. An intake stroke, which starts when the piston is at TDC, ends when the piston is at BDC and draws fresh air into the mixture[4] along the way. In this phase, and in order to increase the amount of air getting sucked into the cylinder, the intake valve opens shortly before the start of the stroke and closes shortly after its' end.
2. A compression stroke, that happens when both valves are closed and the piston is moving upwards in the cylinder, compressing the mixture into a small fraction of its original volume. Near the end of this stroke, combustion will be initiated (by means of a spark plug if it's an SI engine or by means of high compression if it's a CI engine) and the pressure inside the cylinder sharply rises.
3. An expansion stroke, which starts once the piston is at TDC and the high-pressure, high-temperature gases push it downwards, forcing the crankshaft to rotate. As the piston approaches BDC (where the stroke will end), the exhaust valve opens to start the exhaust process and force the pressure inside the cylinder to drop.
4. An exhaust stroke, where the remaining burnt gases exit the cylinder through the opening provided by the exhaust valve, due to the difference in pressure inside and outside the cylinder and to the upwards movement of the piston towards TDC. Once the piston

[3] ICEs can be classified according to a lot of different categories, such as ignition type and cylinder configuration.
[4] Assuming the fuel injection is direct, the injector will send the fuel directly into the cylinder, if it is indirect, then the air getting inside the cylinder in the first stroke will already be mixed with fuel, injected into a chamber before the intake valve.

approaches TDC, the intake valve opens and just after TDC the exhaust valve closes[5], starting the cycle again.

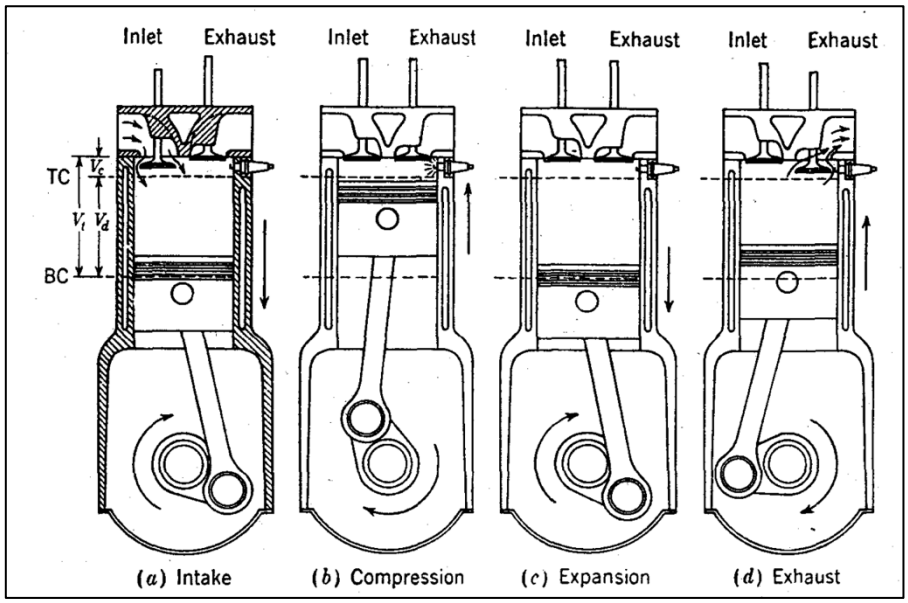

Figure 2.5 - Operating cycle of a four-stroke SI engine [1]

2.2.2.2 Two-Stroke Engines

The two-stroke cycle was developed in order to obtain a higher power output from a given engine size with no need for a valve train and, like the four-stroke cycle, can be used with both SI and CI engines.

In this section, we will analyse the simpler form of the two-stroke engine design, in which the ports in the cylinder are opened and closed by the piston movement and control the intake and exhaust flows while the piston is close to BDC (see Figure 2.6)

This cycle contains the following phases [6]:

1. A compression stroke, which begins once the piston covers both the intake and exhaust ports and then compresses the air/fuel mixture while moving towards TDC, point at which the combustion is initiated. As the piston is moving upwards in the cylinder, besides compressing the mixture, it also draws new mixture into the crankcase, through a spring valve.
2. An expansion stroke, which is similar to that of the four-stroke cycle one while the piston approaches BDC, point at which the exhaust port is first uncovered, in order to let the burnt gases out, followed by the intake port, in order to let the air being compressed inside the crankcase to flow through the transfer port and into the cylinder. Both the piston and the ports are shaped so that the fresh mixture doesn't flow directly out through the exhaust port.

[5] Both the intake and exhaust valves are open at the same time for a short period of time, this phenomenon is called valve overlapping and will be addressed further ahead in this document.

In this case, each engine cycle is completed with only one crankshaft revolution, as opposed to the four-stroke cycle. However, it is almost impossible to completely fill the displaced charge with the new mixture, and some of it always ends up flowing directly through the exhaust port.

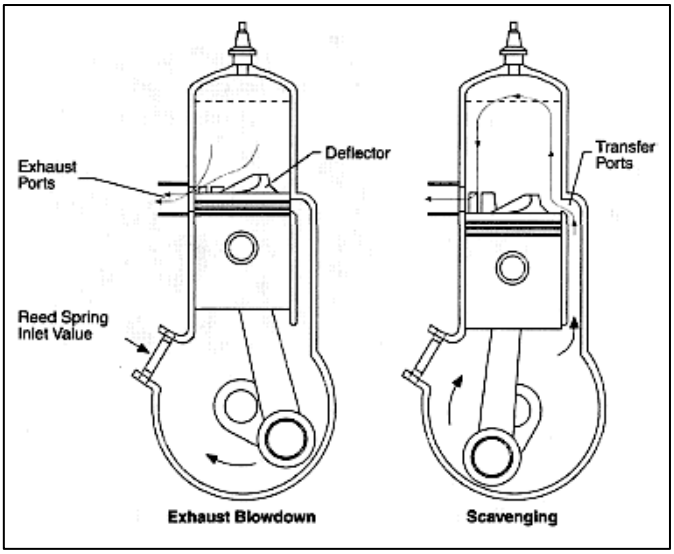

Figure 2.6 - Cross-scavenged designed two-stroke SI engine [6]

2.3 Camshaft and Valve Train

A camshaft can be described as a rod, comprised with one or more cam lobes (cams), that rotates and slides against a piece of machinery (usually named "follower") in order to turn rotational motion into linear motion. This change in motion is achieved due to the cam lobes moving closer and further from the axis of rotation, making the follower travel a certain distance, which is called throw or lift [7]. Valve lift is one of the most important variables when it comes to engine performance, due to the fact that it dictates how long the valves stay open for, the amount of overlap[6] between the intake and exhaust valves, the amount of air, fuel and mixture going in and out of the cylinder, etc.

The working mechanism behind this process is fairly simple: the crankshaft rotates, a timing belt[7] makes it possible, through belt tensioners and sprockets, for the camshaft to rotate as well, but with half the crankshaft's rotational speed. The rotation of the camshaft controls the opening and closing of the intake and exhaust valves, either directly through tappets (Figure 2.7 on the left), or through

[6] Valve overlap happens when both the intake and exhaust valves are open at the same time. This concept will be explained in more depth further ahead.

[7] A timing belt, belt tensioners and sprockets are one example of the many ways to connect a crankshaft to a camshaft.

pushrods and rocker arms (Figure 2.7 on the right) [8]. Seeing as the valves control the amount of air, fuel and mixture going in and out of the cylinder, changing the amount of time that those valves stay open for and/or the point at which they open and close will then change the performance output of the engine itself (SFC, power output, etc.). The process described above of mechanically or electronically manipulating engine valve operations is called Variable Valve Timing (VVT) and it's a concept that has existed for quite some time now, especially when it comes to the automotive industry, and it is further elucidated in Section 2.5.

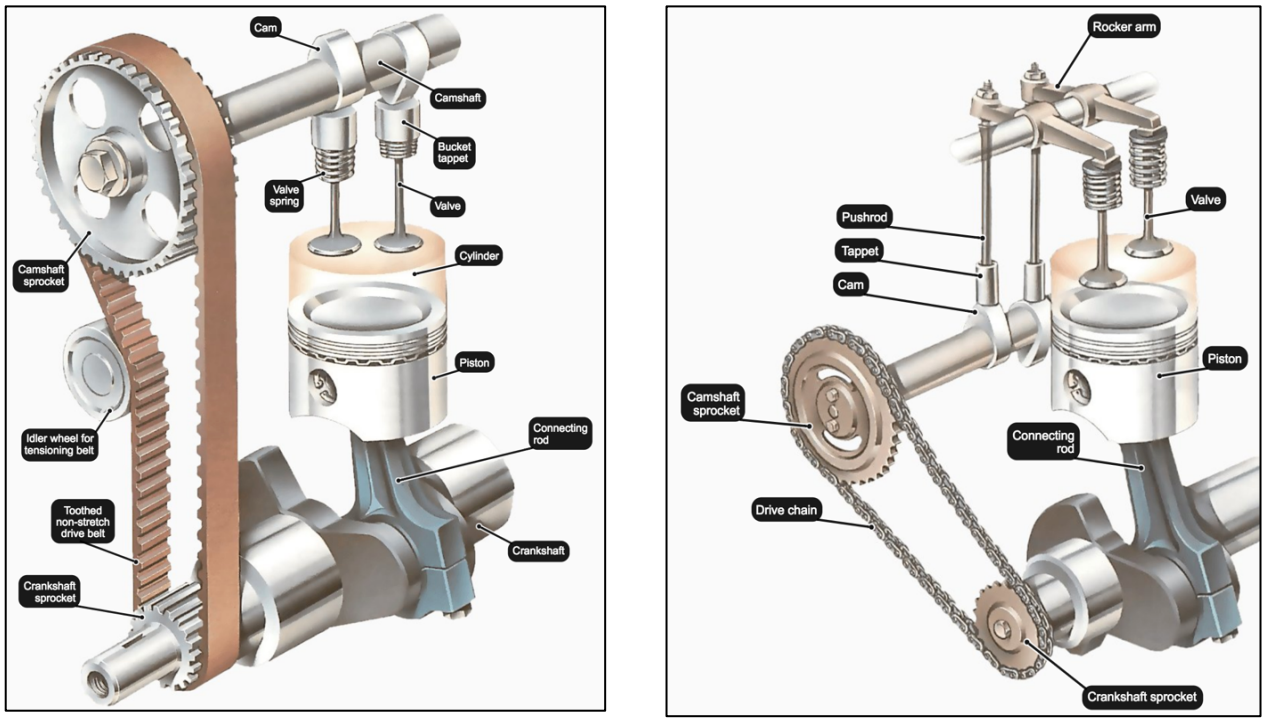

Figure 2.7 - On the left, a crankshaft and camshaft with bucket tappets configuration and, on the right, a crankshaft and camshaft with pushrods and rocker arms configuration [8]

2.4 Cam-follower system classification

Usually, the system that links the cam and the follower is known as the cam-follower system or mechanism, and due to the wide range of applications they can be implemented upon, the need to create new geometries, profiles, and mechanisms aroused. This diversity when it comes to designing cam systems also derives from their versatility and flexibility, which leads to a need for a classification to be made [9]. In this section will be mentioned the different classifications given to cam-follower systems, detailing the most used ones, and even though different nomenclatures are given by different authors, one can focus mainly on the classifications given both by Shigley, J. (1981) and by Norton, R. L. (1999).

2.4.1 According to cam shape

When it comes to cams, they are usually named after their shapes, and the four most usual denominations are: radial cams (Figure 2.8 (a)), wedge cams (Figure 2.8 (b)), cylindrical cams (Figure 2.8 (c)) and face cams (Figure 2.8 (d)). The most common of the mentioned types of cam is the plate radial cam, opposite to the wedge cam, which is not that common, due to the need for a reciprocating movement, not a continuous one [9]. Furthermore, and since the radial cam is the most relevant one for this particular project, we shall henceforth only mention the cam-follower systems that are comprised of radial cams.

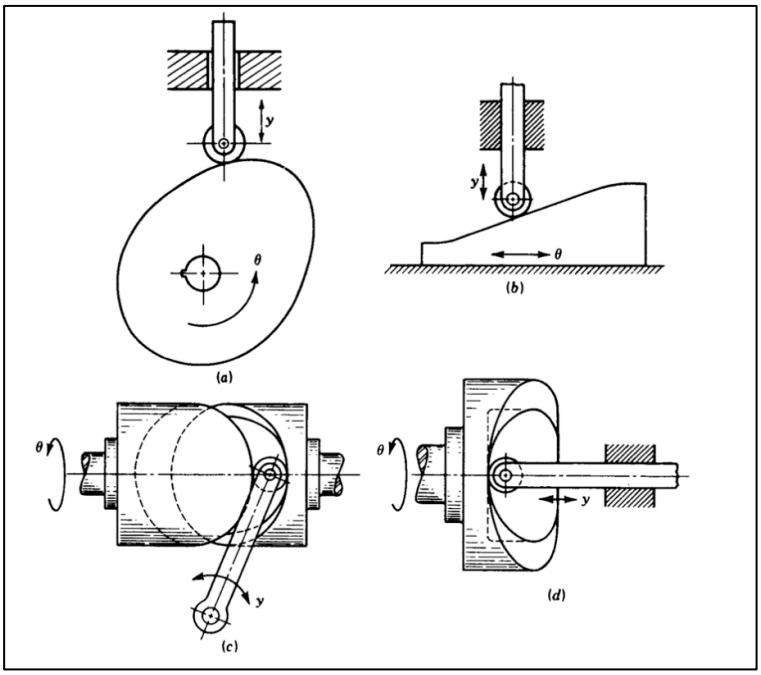

Figure 2.8 - (a) Radial cam; (b) Wedge cam; (c) Cylindrical cam; (d) Face cam. [9]

2.4.2 According to follower design

Having mentioned the different types of cams, it is also relevant to mention the different types of followers that have been developed over the years to couple with different cams. As with the previous classification, the follower shape can also be used to classify cam-follower systems, and, like it has been mentioned, only follower shapes that are compatible with radial cams will be discussed. There are four main categories used to classify followers by shape: the knife-edge follower (Figure 2.9 (a)), the flat-faced follower (Figure 2.9 (b)), the roller follower (Figure 2.9 (c)) and the curved-shoe follower (Figure 2.9 (d)) [9]. In the next section, more information will be given as to the different follower motions observed in Figure 2.9, which can also be used to classify, together with the present section, different cam-follower systems.

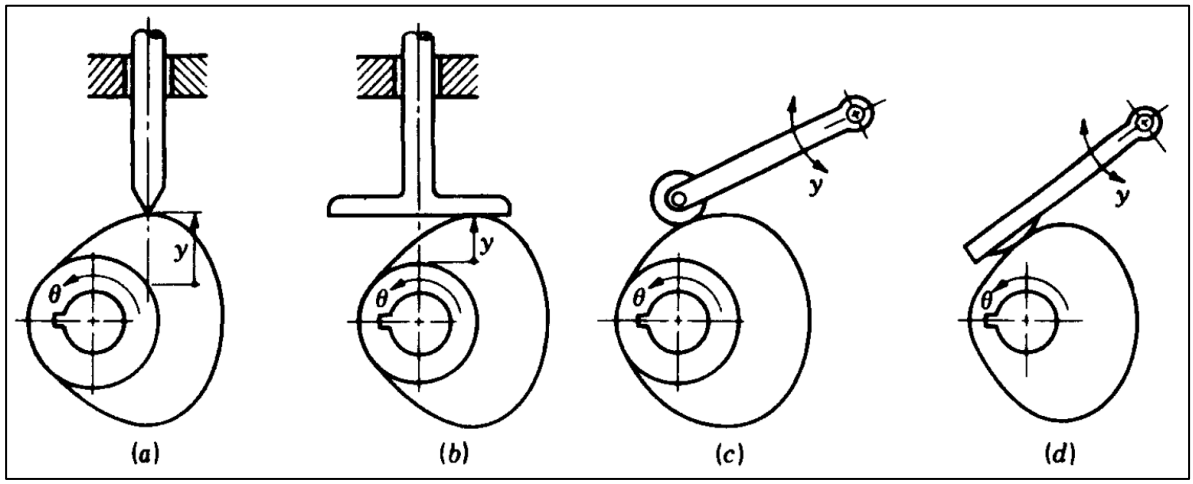

Figure 2.9 – (a) Knife-edge follower; (b) Flat-faced follower; (c) Roller follower; (d) Curved-shoe follower [9].

2.4.3 According to follower motion

Besides shape and geometry, followers can also be divided into different classifications when it comes to their motion patterns, with the two main groups being: oscillating followers (Figure 2.10) and translating followers (Figure 2.11). Both configurations are equivalents of four-bar mechanisms at any instantaneous position, but with much more versatility and flexibility, due to the fact that, as opposed to rigid four-bar linkages and mechanisms, the "imaginary" linkages in cam-follower systems have different lengths throughout the different rotation positions. [10]

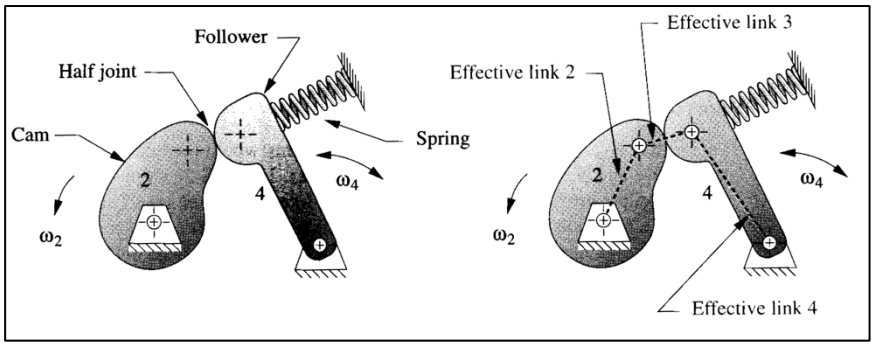

Figure 2.10 - Oscillating follower and the equivalent four-bar mechanism it represents. [10]

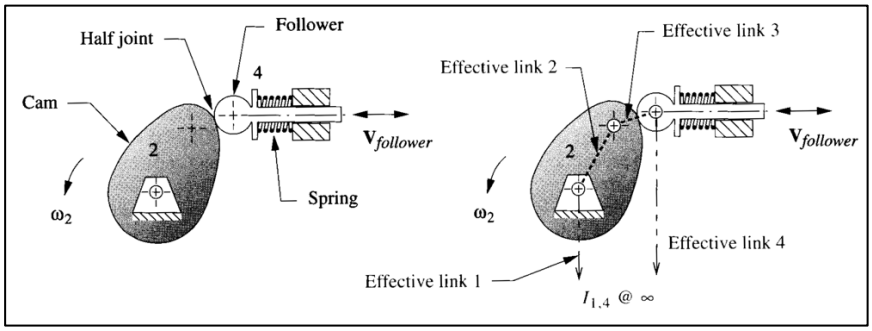

Figure 2.11 - Translating follower and the equivalent four-bar mechanism it represents. [10]

2.5 Variable Valve Timing (VVT)

In this section, a brief explanation of different VVT systems will be given, in order to understand the effects of having different timings and durations when it comes to an engine valve train and cam-follower systems. The first and most primitive form of VVT came into existence in the 19th century, incorporated in steam engines. The early steam locomotives had a system called the Stephenson valve gear, which was able to support variable cut-off of steam admission to the cylinders during the power stroke [11]. Later, and with the evolution of technology, more sophisticated VVT systems were created.

2.5.1 Honda's VTEC system

Probably one of the best VVT systems of all time, that is still used to this day, is the Honda VTEC (Variable Valve Timing & Lift Electronic Control) system which, appearing in 1990, was definitely the first one to be commercially successful and allowed the manufacturer, at the time, to produce the B16A automotive engine series, comprised of 1600 cm^3, four-cylinder engines that produced up to 160 horsepower [12]. These specifications are impressive, even by today's standards and carved a path through which Honda would come to be very successful. Engines that had the VTEC system (see Fig.2.12), as opposed to other ICEs, were comprised of three cams and three rocker arms for every two (intake or exhaust) valves. Two of those cams are regular ones that operate the valves alone at low engine speeds, optimizing fuel consumption, while the third one is only activated at higher engine speeds (usually 4000-5000 rpm) through a high-pressure oil circuit and a solenoid, working jointly with the other two cams and rocker arms to enhance the engine's performance, due to the fact that the middle cam is larger than the other two [12]. This means the valves had higher lift and for longer periods of time. As opposed to other car manufacturers, Honda created a system that could vary not only the timing and duration of the valves but also the lift, which was unheard of at the time.

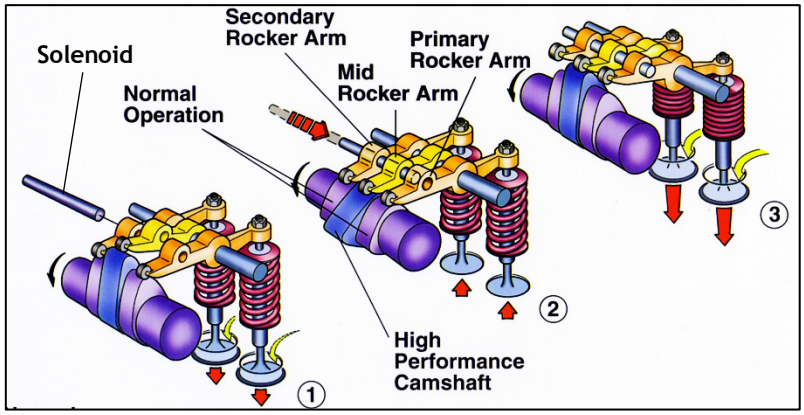

Figure 2.12 – Adapted representation of the VTEC system, in which (1) is the low rpm operation, (2) is the transition in which the solenoid is being engaged and (3) is the high rpm operation, with all three cams working jointly [13].

2.6 Cam design curves and diagrams

In this section will be mentioned some of the different ways to create and study cam curves and diagrams, as well as some of the different types that exist and their suitableness when it comes to this particular project. Due to the fact that cam design is a very complex subject, with a lot of different variables and a big mechanical background, an attempt will be made of narrowing it down to the most important concepts for this project without leaving out any crucial information.

When attempting to design a cam profile, some criteria must be met in order for the profile to be suitable for fabrication. First and foremost, it has to obey the fundamental law of cam design and its respective corollary, which state that any cam designed for operation at other than very low speeds must have continuous functions through the first and second derivatives of displacement (velocity and acceleration, respectively) across the entire interval (360 degrees) and also that the jerk function (third derivative of the displacement function) must be finite across the entire interval (360 degrees) [10].

The displacement (s), velocity (v), acceleration (a), and jerk (j) functions mentioned above are crucial when it comes to designing a cam, since they are used to describe the behaviour of the cam--follower system, throughout one revolution of the engine, in which it's possible to discern a portion of the displacement curve that goes from zero to the maximum lift point (this is called the rise), another that goes from the maximum lift point to zero (this is called the fall or return) and a third portion in which the lift is constant (this is called the dwell) [9].

The s, v, a and j function curves are usually plotted together to form what is called the s-v-a-j diagram, from which it is possible to understand if the cam being studied obeys, or not, the fundamental law of cam design and its corollary, as will be shown in the next sub-section.

2.6.1 Simple harmonic motion curve

One of the most popular curves in the literature is the simple harmonic motion curve. It is one of the standard cam curves and is usually acceptable because the base functions behind it are either sine or cosine functions, which remain continuous throughout any number of differentiations, thus complying with the fundamental law of cam design [10]. The equations for a simple harmonic rise motion are as follows:

$$s = \frac{L}{2}\left[1 - \cos(\pi\frac{\theta}{\beta})\right] \tag{2.1}$$

$$v = \frac{\pi}{\beta}\frac{L}{2}\sin(\pi\frac{\theta}{\beta}) \tag{2.2}$$

$$a = \frac{\pi^2 L}{\beta^2 2}\cos(\pi\frac{\theta}{\beta}) \tag{2.3}$$

$$j = -\frac{\pi^3 L}{\beta^3 2}\sin(\pi\frac{\theta}{\beta}) \tag{2.4}$$

where L is the maximum lift, θ is the camshaft angle and β is the total angle of the rise segment [9].

After plotting the s-v-a-j diagram for the simple harmonic motion shown in figure 2.8[8], it is clearly possible to see that the fundamental law of cam design is complied with but, on the other hand, the third derivative is infinite on the nighbouring points of both ends of the curve, which means that the corollary for the fundamental law is not verified.

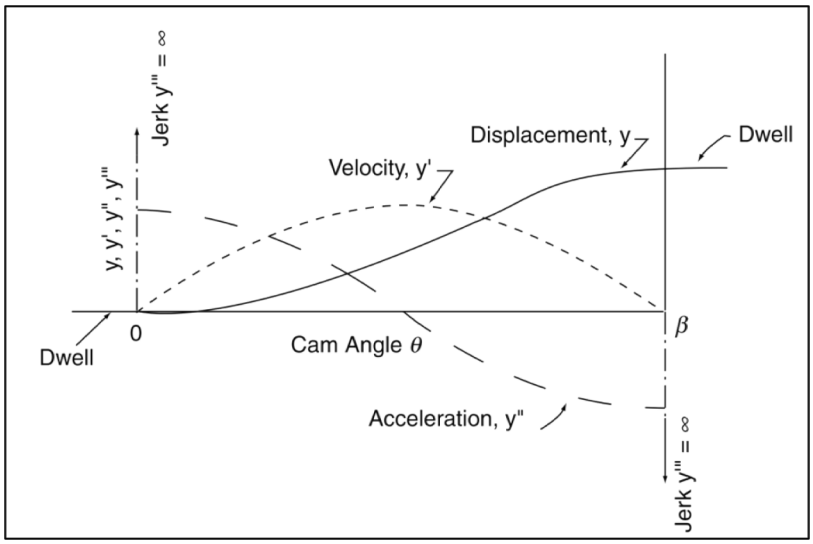

Figure 2.13 - Simple harmonic motion diagram [14]

Despite the fact that the simple harmonic motion curve can seem appealing due to the fact that some of the fundamental criteria are easily met, the corollary of the fundamental law of cam design is not met and the second derivative of the displacement isn't zero at the beginning and ending of the motion. What this means is that this motion curve cannot be used (at least by itself) to accurately predict the behaviour of the cam-follower system and is, therefore, not suitable for high-speed movements. In the next section will be mentioned the combined motion curves, with the main goal being to reduce the acceleration values and variations in order for the cam to be reliable and not damage any engine components during rotation. These combined motion functions may also prove to be more accurate than the standard ones.

[8] It is possible to observe that the nomenclature used by Rothbart, Harold A. (2004) indicates that instead of s,v,a and j, the author has opted to use y, y', y'' and y''', which is also correct.

2.6.2 Combined functions

Combined motion functions are usually appealing to cam designers due to the fact that they combine diverse basic motion functions into one, meaning it is more accurate and less likely to fail the strict cam design criteria, while still having some adjacent simplicity to them. As a general rule of thumb, when designing a cam, one must focus on reducing the acceleration values and their variation, and from this comes the modified trapezoidal acceleration. This function is a combination of both the sine acceleration curve and the constant acceleration one, which means that a full period sine wave is "cut" into fourths and "placed into" the square, constant acceleration curve, which creates a smooth transition from the functions' zeros to the maximum and minimum values of the function) [10].

There is a wide variety of combined functions the cam designer can choose from, however, for the sake of reducing the document size, these will not be deduced and specified in this particular document, also due to the lack of interest of these functions for this specific project.

2.6.3 Polynomial functions

Although the standard and combined cam functions mentioned before (and a wide variety of others) are usually adequate if accurately dimensioned, they certainly don't represent the whole picture when it comes to cam design functions. It is often common to opt to create polynomial motion curves, due to the fact that these are very versatile and can, therefore, be tailored to the designer's wish [9]. The general form of the polynomial motion equation is as follows:

$$s = C_0 + C_1x + C_2x^2 + C_3x^3 + C_4x^4 + C_5x^5 + C_6x^6 + \cdots + C_nx^n \tag{2.5}$$

with s being the follower displacement, x being the independent variable which, in our case, is going to be θ/β, and finally C_n being the unknown constant coefficients which will be found to fulfil the requirements of a specific design [10]. The degree of the polynomial function to be used is going to be determined by the number of boundary conditions (or BCs) specified at the beginning of the design process with the following relation:

$$n = BC's - 1 \tag{2.6}$$

where the BCs will be specific points, chosen by the designer, throughout the s-v-a-j diagram in order to tailor the resulting curves to the desired end.

Since the BCs are going to be the parameters that dictate the number of variables of the polynomial equation, the first step to accurately create the desired curve is to specify the BCs keeping in mind

the final objective. As an example, As an example, a 3-4-5-6 polynomial function will be created by using two segments of BCs, one for the rise-fall ($\theta = 0$ and $\theta = \beta$) and another for the dwell ($\theta = \beta/2$), as in Table 2.1:

Table 2.1 - Boundary conditions for a 3-4-5-6 polynomial

Position of θ according to β	Boundary Conditions		
θ = 0	s=0	v=0	a=0
θ = β/2	s=L		
θ = β	s=0	v=0	a=0

which means, by having 7 BCs, according to equation (2.6), the polynomial equation to be created will have a degree of 6, is the aim of in this example. If the independent variable is then replaced in equation (2.5) for θ/β, the latter becomes:

$$s = C_0 + C_1\left(\frac{\theta}{\beta}\right) + C_2\left(\frac{\theta}{\beta}\right)^2 + C_3\left(\frac{\theta}{\beta}\right)^3 + C_4\left(\frac{\theta}{\beta}\right)^4 + C_5\left(\frac{\theta}{\beta}\right)^5 + C_6\left(\frac{\theta}{\beta}\right)^6 \quad (2.7)$$

and consequently, the first, second and third derivatives become:

$$v = \frac{1}{\beta}\left[C_1 + 2C_2\left(\frac{\theta}{\beta}\right) + 3C_3\left(\frac{\theta}{\beta}\right)^2 + 4C_4\left(\frac{\theta}{\beta}\right)^3 + 5C_5\left(\frac{\theta}{\beta}\right)^4 + 6C_6\left(\frac{\theta}{\beta}\right)^5\right] \quad (2.8)$$

$$a = \frac{1}{\beta^2}\left[2C_2 + 6C_3\left(\frac{\theta}{\beta}\right) + 12C_4\left(\frac{\theta}{\beta}\right)^2 + 20C_5\left(\frac{\theta}{\beta}\right)^3 + 30C_6\left(\frac{\theta}{\beta}\right)^4\right] \quad (2.9)$$

$$j = \frac{1}{\beta^3}\left[6C_3 + 24C_4\left(\frac{\theta}{\beta}\right) + 60C_5\left(\frac{\theta}{\beta}\right)^2 + 120C_6\left(\frac{\theta}{\beta}\right)^3\right] \quad (2.10)$$

keeping in mind that, since the jerk is not constrained in the boundary conditions, it won't be necessary to use equation (2.10) to find the constant coefficients.

Having found the necessary derivatives, then one has to substitute the BCs shown in Table 2.1 in equations (2.7), (2.8) and (2.9) in order to solve for the constant coefficients. Starting with the first set of BCs specified:

θ = 0	s=0	v=0	a=0

it can be seen firstly that when θ=0, s=0 and as so, by substituting these values in equation (2.7), one obtains:

$$0 = C_0 + C_1\left(\frac{0}{\beta}\right) + C_2\left(\frac{0}{\beta}\right)^2 + C_3\left(\frac{0}{\beta}\right)^3 + C_4\left(\frac{0}{\beta}\right)^4 + C_5\left(\frac{0}{\beta}\right)^5 + C_6\left(\frac{0}{\beta}\right)^6 \Leftrightarrow$$

$$\Leftrightarrow C_0 = 0 \tag{2.11}$$

therefore, by repeating this process for v=0 in equation (2.8) and a=0 in equation (2.9), the results are respectively:

$$0 = \frac{1}{\beta}\left[C_1 + 2C_2(\frac{0}{\beta}) + 3C_3(\frac{0}{\beta})^2 + 4C_4(\frac{0}{\beta})^3 + 5C_5(\frac{0}{\beta})^4 + 6C_6(\frac{0}{\beta})^5\right] \Leftrightarrow$$

$$\Leftrightarrow C_1 = 0 \tag{2.12}$$

and

$$0 = \frac{1}{\beta^2}\left[2C_2 + 6C_3(\frac{0}{\beta}) + 12C_4(\frac{0}{\beta})^2 + 20C_5(\frac{0}{\beta})^3 + 30C_6(\frac{0}{\beta})^4\right] \Leftrightarrow$$

$$\Leftrightarrow C_2 = 0 \tag{2.13}$$

and so, after analysing the first set of BCs, the values of the first three constant coefficients are obtained.

Only four unknown coefficients remain, and the previous calculation process will be repeated for the last set of four BCs, in order to obtain four new equations to solve simultaneously:

θ = β/2	s=L		
θ = β	s=0	v=0	a=0

Substituting the first BC in equation (2.7) gives:

$$L = C_3(\frac{1}{2})^3 + C_4(\frac{1}{2})^4 + C_5(\frac{1}{2})^5 + C_6(\frac{1}{2})^6 \Leftrightarrow$$

$$\Leftrightarrow L = C_3\frac{1}{8} + C_4\frac{1}{16} + C_5\frac{1}{32} + C_6\frac{1}{64} \tag{2.14}$$

and repeating the same process for the last three BCs, when $\theta = \beta$, in equations (2.7), (2.8) and (2.9) respectively:

$$\Leftrightarrow C_3 + C_4 + C_5 + C_6 = 0 \tag{2.15}$$

$$\Leftrightarrow \frac{1}{\beta}(3C_3 + 4C_4 + 5C_5 + 6C_6) = 0 \quad (2.16)$$

$$\Leftrightarrow \frac{1}{\beta^2}[6C_3 + 12C_4 + 20C_5 + 30C_6] = 0 \quad (2.17)$$

Finally, having found four equations to solve for the four unknown constant coefficients, with resource to any calculator or computer that contains a matrix solving function, it is possible to find the four coefficients simultaneously, by putting equations (2.14), (2.15), (2,16) and (2.17) into a matrix and solving for the unknown coefficients:

$$\begin{bmatrix} \frac{1}{8} & \frac{1}{16} & \frac{1}{32} & \frac{1}{64} \\ 1 & 1 & 1 & 1 \\ 3x & 4x & 5x & 6x \\ 6x^2 & 12x^2 & 20x^2 & 30x^2 \end{bmatrix} \begin{bmatrix} C_3 \\ C_4 \\ C_5 \\ C_6 \end{bmatrix} = \begin{bmatrix} L \\ 0 \\ 0 \\ 0 \end{bmatrix}, \text{with } x = \frac{1}{\beta}$$

$$\begin{cases} C_3 = 64L \\ C_4 = -192L \\ C_5 = 192L \\ C_6 = -64L \end{cases}, \text{with } \beta \neq 0$$

Since the first three constant coefficients were already known from equations (2.11), (2.12) and (2.13), the 3-4-5-6 polynomial and its' three derivatives can now be obtained by substituting the constant coefficients in equations (2.7), (2.8), (2.9) and (2.10):

$$s = L\left[64(\frac{\theta}{\beta})^3 - 192\left(\frac{\theta}{\beta}\right)^4 + 192\left(\frac{\theta}{\beta}\right)^5 - 64\left(\frac{\theta}{\beta}\right)^6\right] \quad (2.18)$$

$$v = \frac{L}{\beta}\left[192(\frac{\theta}{\beta})^2 - 768\left(\frac{\theta}{\beta}\right)^3 + 960\left(\frac{\theta}{\beta}\right)^4 - 384\left(\frac{\theta}{\beta}\right)^5\right] \quad (2.19)$$

$$a = \frac{L}{\beta^2}\left[384\left(\frac{\theta}{\beta}\right) - 2304\left(\frac{\theta}{\beta}\right)^2 + 3840\left(\frac{\theta}{\beta}\right)^3 - 1920\left(\frac{\theta}{\beta}\right)^4\right] \quad (2.20)$$

$$j = \frac{L}{\beta^3}\left[384 - 4608\left(\frac{\theta}{\beta}\right) + 11520\left(\frac{\theta}{\beta}\right)^2 - 7680\left(\frac{\theta}{\beta}\right)^3\right] \quad (2.21)$$

The plot of these four equations, considering β=360º, $\theta \in$[0º;360º] and L=3mm[9] is presented at Fig. 2.14.

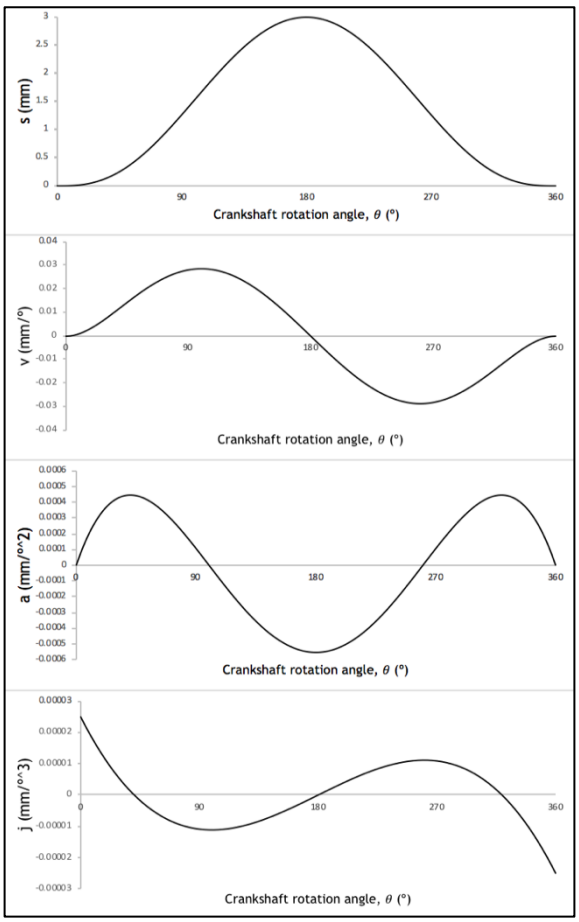

Figure 2.14 - Smoothed curve scatter plots created in the Microsoft Excel software for the 3-4-5-6 polynomial described in this sub-section.

In Figure 2.14 it is possible to graphically confirm that there are no discontinuities in the displacement, velocity and acceleration functions and that the jerk function is finite throughout the entire interval, thus confirming that both the fundamental law of cam design and its' corollary are complied with.

Although there is a very wide variety of functions to choose from, including even more versatile versions of the polynomial functions mentioned in this subsection, called spline functions [14], due to the fact that for this particular project they have no interest, the criteria and derivation procedure will not be specified like for the polynomial functions. Furthermore, it's important to note that polynomial functions can accurately predict the behaviour of the cam-follower system at the BCs but, there is no telling if they will have the desired behaviour in between those points. This is

[9] These are only example values; all of the mentioned variables can have whichever values the designer requires.

especially true for higher degree polynomials, which is why the best approach when attempting to find an accurate function is to try and minimize the number of BCs used for the curves to fit the designer's needs.

Chapter 3

Cam Design

3.1 Valve lift measurement

In order to accurately dimension the new cam, the first step is to get to know the original one of the Honda GX31 (the full engine specifications can be found in Table A.1 of Appendix A), which means a study about the valve lift, velocity, acceleration and jerk will have to be made.
When it comes to the valve lift, a practical approach has been taken, with the experimental procedure being as follows:

- Firstly, a graduated disk was created, utilizing the software CATIAV5 (Fig. B.1 of Appendix B), in which the scale was from 0º to 360º[10], with 2º intervals;
- The disk was then printed and coupled to a round, wooden plank which was, afterwards, perforated with a drill in order to couple the disk to the engine through means of two screws;
- The engine is then locked in place by a mechanical vice and the disk coupled to the engine ;
- When coupling the disk to the engine, it's important to make sure the 0º mark is coincident with the TDC (which can be easily located by removing the spark plug and checking when the piston is at the top of the cylinder before the exhaust valve opens and then align a little cut on one of the flywheel fins with a metallic pin on the cylinder block, and it's also important to pinpoint the location which is used as a reference for the degree measurement, when rotating the flywheel and the disk;
- Once the engine is locked in place, the valve cover is removed in order to reach the rocker arms and, through means of a feeler gauge, both the intake and exhaust valve clearances are set according to the manufacturers' specifications (Table A.1 of Appendix A);
- The next step in the process is, still keeping the valve cover removed, to mount the valve lift measuring apparatus, which consists of a magnetic-based mechanical arm, placed at the base of the mechanical vice, and an analogical dial indicator mounted on the non-magnetic end of the mechanical arm with the probe tip resting on the valve spring. Since the dial indicator will be used to measure the amount of valve displacement (lift), it's important to make sure it is completely vertical to minimize the measurement errors;
- Once the apparatus is fully mounted and functional (see Figure B.2 of appendix B), the measurements start taking place, beginning with the intake valve. With the disk set at 0º, it is then slowly rotated, by hand, anti-clockwise and once the first movement is seen on the

[10] This scale is used due to the fact that this measurement is being made for the CA and not cA.

dial indicator, the value of the lift is written down, that point is considered to be the IVO and from that point onwards, every 2° increment results in a valve lift change, which is written down. This process continues until the valve lift reaches 0 mm again, this point is considered to be the IVC and marks the end of the measurements for the intake valve lift;

- The latter process is repeated for the exhaust valve and this means that all the measured values can be plotted into a scatter point chart in the Microsoft Excel software, giving a rough approximation of the valve lift curves (Figure 3.1).

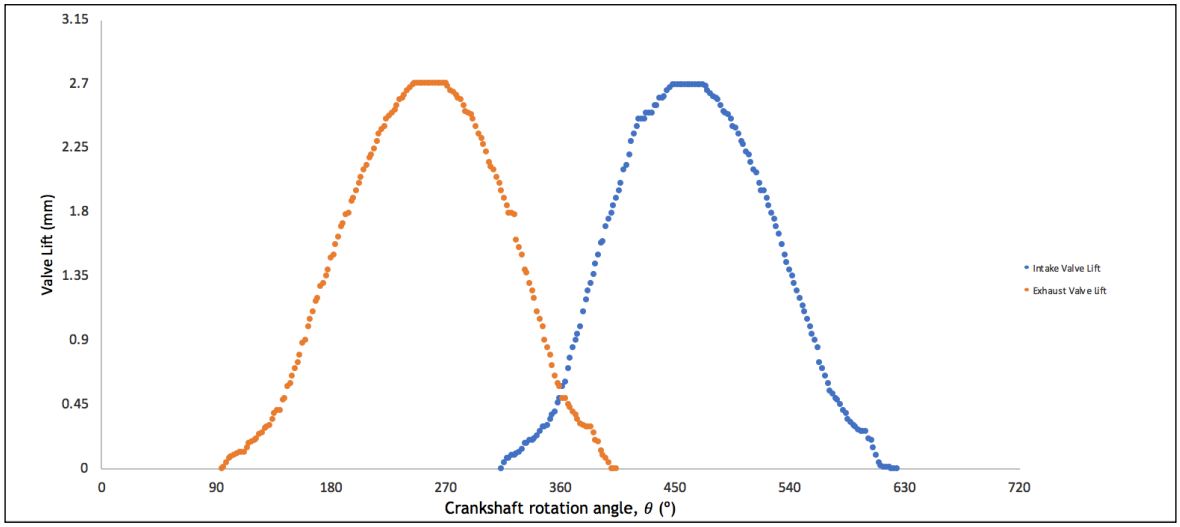

Figure 3.1 - Scatter point chart of the valve lift measurements, in relation to CA.

In the valve displacement chart displayed in Fig. 3.1, it's possible to observe some unusual characteristics when it comes to measurement precision. Firstly, it's important to recognize that the analogic dial indicator used is a very sensitive piece of equipment, due to the fact that the scale is so small (maximum of 10 mm with 0,1 mm intervals) and what this means is that, even though the procedure has been carried out with extreme care to avoid any lack of precision, any small disturbance to the apparatus environment will cause a less accurate measurement. Furthermore, the lack of precision seen is also caused by a compression release mechanism incorporated to the camshaft that is used to ease a cold starting of the engine, by raising the follower through means of a machined metal pin, not letting the exhaust valve close under a certain engine speed, and therefore releasing the compression inside the cylinder so that the engine can start without having to work against the pumping of the piston.

Table 3.1 shows the values that can be read in the plotted measurements in Figure 3.1.:

Table 3.1 - Measured valve specifications, according to the CA, for the Honda GX31

IVO (°)	300
IVC (°)	630[11]

[11] Due to the measurement imprecisions mentioned in this section, the values of both the IVC and EVC were read in the polynomial approximation curve shown in the next section.

EVO (°)	91
EVC (°)	421
Valve Duration (°)	330
Valve Overlap (°)	121
Valve Gap at Maximum Lift (°)	196
Maximum Lift (mm)	2.7

3.2 Lift curve approximation and s-v-a-j diagram

In this section will be mentioned the procedure that was followed in order to solve and plot the polynomial equation that follows approximately the same pattern as the measured lift curve, shown in the prior section of this chapter. As it has been in Chapter 2, there is a wide variety of curves that can be used to describe valve movements in ICEs, and it's usually possible to simply adapt those curves to the desired situation by changing the BCs of the system. In this case, however, it was decided that a new curve should be created for the lift (and consequently the velocity, acceleration and jerk) since this would mean that the full range of the curve (rise, fall and dwell) could be incorporated into a single set of equations.

The process for the creation of the polynomial motion curve is the same that was demonstrated in Section 2.5.3 of this dissertation, with the exception of the values of β which will be equal to the valve duration shown in Table 3.1 (β=330°), θ which will range from the beginning to the end of the valve duration interval ($\theta \in$[91°;421°] for the exhaust valve and $\theta \in$[314;644°] for the intake valve) and the maximum lift which will be equal to the measured one (L=2,7mm). The first step is to define the BCs as it was done in Section 2.6.3:

Table 3.2 - Boundary conditions in order to obtain a 3-4-5-6 polynomial function

Position of θ according to β	Boundary Conditions		
θ = 0	s=0	v=0	a=0
θ = β/2	s=L		
θ = β	s=0	v=0	a=0

which, as it's possible to observe in Table 3.2, are exactly the same as Table 2.1, since the constraints desired for this polynomial function are the same as the one used as an example in Section 2.5.3. What this means is that the final motion equations will be the same as equations (2.18-2.21) which will then be modified to fit the measured values of this specific system and, if the resulting displacement curve doesn't adapt accurately to the measured curves in Figure 3.1, one must keep adding BCs until the resulting curve is satisfactory. Having said this, the values of β and L are substituted in equations (2.18-2.21), obtaining:

$$s = 2{,}7\left[64\left(\frac{\theta}{330}\right)^3 - 192\left(\frac{\theta}{330}\right)^4 + 192\left(\frac{\theta}{330}\right)^5 - 64\left(\frac{\theta}{330}\right)^6\right] \quad (3.1)$$

$$v = \frac{2{,}7}{330}\left[192\left(\frac{\theta}{330}\right)^2 - 768\left(\frac{\theta}{330}\right)^3 + 960\left(\frac{\theta}{330}\right)^4 - 384\left(\frac{\theta}{330}\right)^5\right] \quad (3.2)$$

$$a = \frac{2{,}7}{330^2}\left[384\left(\frac{\theta}{330}\right) - 2304\left(\frac{\theta}{330}\right)^2 + 3840\left(\frac{\theta}{330}\right)^3 - 1920\left(\frac{\theta}{330}\right)^4\right] \quad (3.3)$$

$$j = \frac{2{,}7}{330^3}\left[384 - 4608\left(\frac{\theta}{330}\right) + 11520\left(\frac{\theta}{330}\right)^2 - 7680\left(\frac{\theta}{330}\right)^3\right] \quad (3.4)$$

and, since the values of θ range from the EVO to the EVC, for the exhaust valve, and from the IVO to the IVC, for the intake valve, the motion curves can be plotted (see Fig. 3.2) together with the measured curves, in order to understand if this sixth-degree polynomial adapts to the measurements.

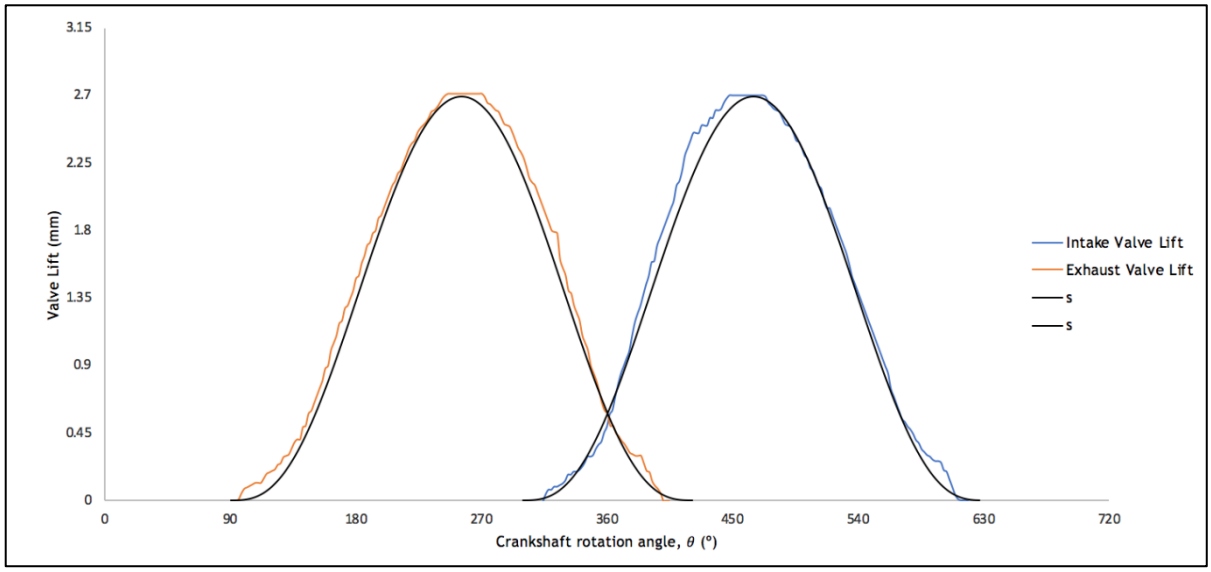

Figure 3.2 - Measured lift curves overlapped with the 3-4-5-6 polynomial motion curves

After having plotted the sixth-degree polynomial curves over the measured ones, it can be seen that they adapt well, albeit not completely accurately, but still accurate enough to avoid having to use a higher-degree function that may cause undesired variations in the motion behaviour. There is still need, however, to verify that the profile of the derivatives is within the acceptable threshold (see Fig. 3.3).

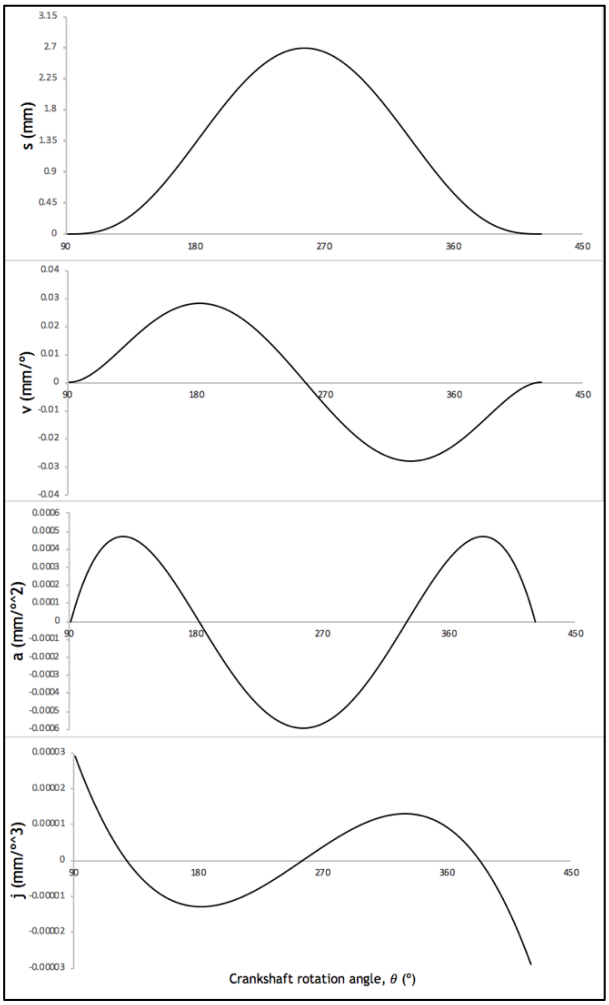

Figure 3.3 - Smoothed curve scatter plots for the s-v-a-j diagrams of the 3-4-5-6 polynomial function

Having plotted the complete s-v-a-j diagram, it can be confirmed that the first and second derivatives are continuous throughout the entire measured interval and that the third derivative is finite throughout the same interval. This means that the polynomial motion function derived in equations (3.1-3.4) can be used to describe the motion behaviour of this particular cam-follower system.

In the next section, the design of the cam-follower system mechanism will be presented, which will be used to allow the creation of a cam profile in the Microsoft Excel software.

3.3 Cam-follower system analysis

As was demonstrated in Section 2.4, there is a wide variety of cam-follower systems available for manufacturers to choose from when conceiving engines or other mechanisms that involve the use of camshafts and followers. However, the cam-follower system in the Honda GX31 is a very unusual and distinctive one, in the sense that it's a mixture of a few different mentioned systems with some unusual characteristics. For this reason, a detailed description of the system's working mechanism will be made and, later in the section, the procedure followed for the creation of the cam profile will be shown and explained.

Next, some photographs will be shown in which it is possible to see the actual mechanism present in the Honda GX31 engine, with a legend to discern each of the crucial components (see Figs. 3.4 to 3.6).

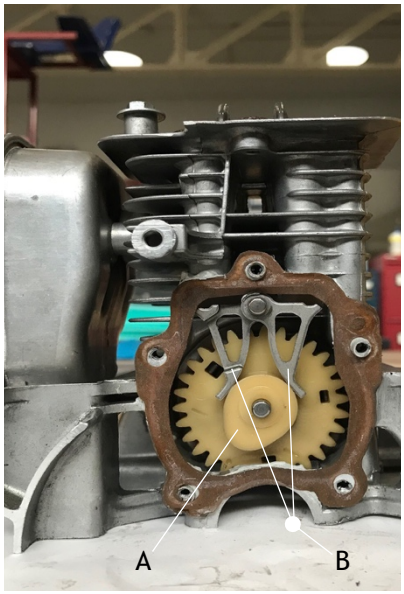

Figure 3.4 - Honda GX31 cam-follower system and partial cylinder block.

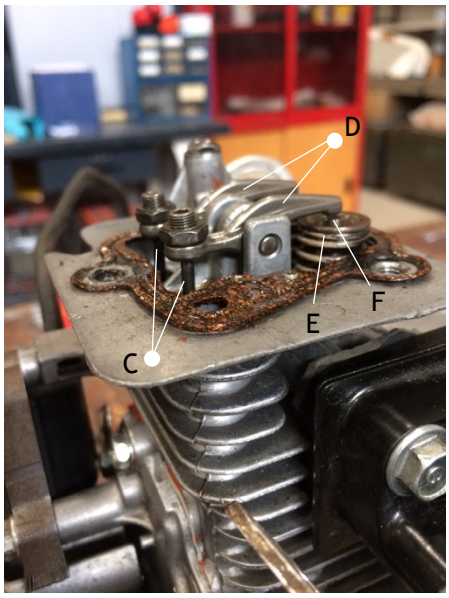

Figure 3.5 - Honda GX31 cylinder head and valve train.

The components shown in Figures 3.4 and 3.5 are as follows:

- **A** – Cam lobe and spur gear that connects to the crankshaft;
- **B** – Followers (for the exhaust valve on the left and for the intake valve on the right);
- **C** – Pushrods that connect the followers to the rocker arms (the one furthest away for the exhaust valve and the one nearest for the intake valve);
- **D** – Rocker arms that translate the follower motion to the valves (the one furthest away for the exhaust valve and the one nearest for the intake valve);

- **E** – Intake valve spring (the exhaust valve spring can't be seen in this picture but it's directly below the exhaust valve rocker arm);
- **F** – Intake valve (the exhaust valve can't be seen in this picture but it's directly below the exhaust valve rocker arm);

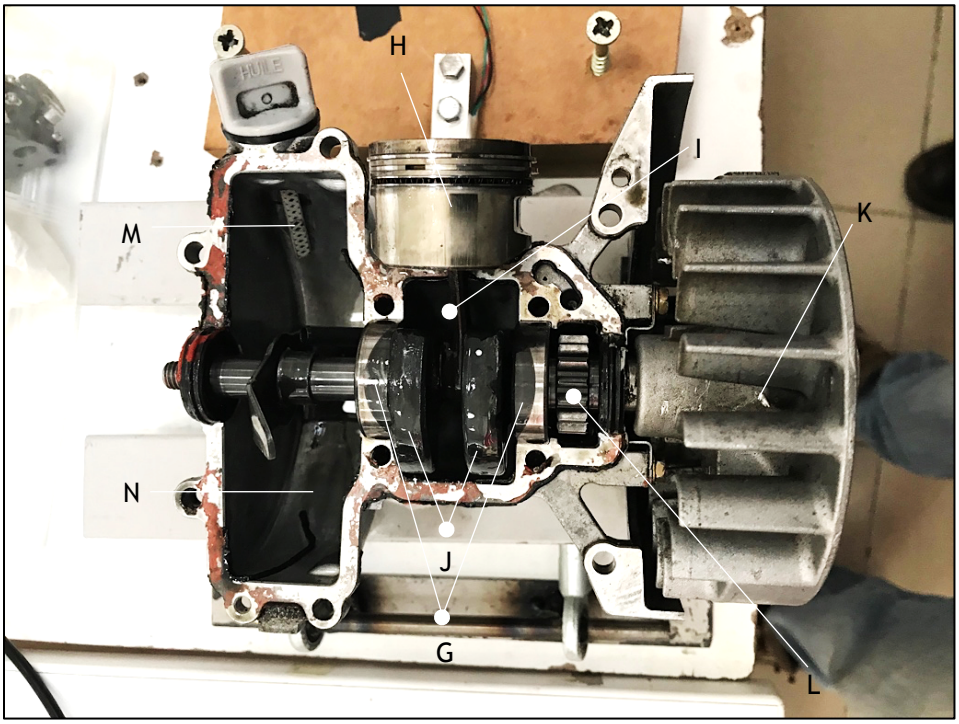

Figure 3.6 - Honda GX31 top-view of the block internal components.

Whereas the components shown in Figure 3.6 are as follows:

- **G** – Crankshaft bearings;
- **H** – Piston;
- **I** – Connecting rod;
- **J** – Crankshaft;
- **K** –Engine flywheel;
- **L** – Spur gear that rotates with the flywheel and connects to spur gear shown in A, making it, and consequently the cam lobe, rotate clockwise;
- **M** – Oil dipstick used to check the engine oil level;
- **N** – Oil pan.

As it is shown in Figure 3.4, there are some unusual characteristics when it comes to this particular cam-follower system: first and foremost, there is a single, egg-shaped cam that controls, through oscillating, curved followers, both the intake and exhaust valves. When it comes to designing a new cam for the engine, this can prove to be a difficult obstacle due to the fact that trying to alter the behaviour of one of the valves will, consequently, alter the behaviour of the other one i.e., if the cam is designed in order to achieve EIVC the first thing to happen is that EEVC is also obtained (which

can be prejudicial in the sense that when the intake valve opens again, there will be residual burned gases still inside the cylinder). The other eventually that will occur is that if only one aspect of the cam-follower mechanism behaviour is altered, an asymmetrical cam profile will be obtained as a result and although this is not unheard of in the cam design subject, it is not usually favourable.

Having said this, the actual geometrical analysis of the system will be presented, in which the first step is to try to photograph the mechanism with a nearby scalar instrument to serve as a benchmark for the image's scale[12], then enlarge the image and print it, so that it is possible to determine the necessary constraints for the designing of the cam profile.

In Figure 3.7 is shown the mentioned image with the measured constraints and variables, in which, when it came to the measurement of the different angles and distances, R_1, R_2, R_3, R_4, R_b, φ and δ_4 were measured using the suitable instruments (R_b was measured directly on the cam with the aid of a Vernier Calliper while φ, δ_4 R_1, R_2, R_3 and R_4 were measured on the enlarged photograph using a digital protractor and a graduated ruler) and, when it came to the distances, all of them were measured in millimetres and divided by 6,8 in order to adapt to the chosen scale, while the angle was measured in degrees. Keeping this in mind, R_1 was considered to be the distance between the centre[13] of the follower locking pin and the position of the base of the intake valve pushrod (which had been removed at the time the photograph was taken), R_2 the distance between the centre of the follower locking pin and the centre of the follower circumference arc depicted in Figure 3.7 (point O), R_3 the distance between the centre of the cam locking pin and point O, R_4 the distance between the centre of the cam locking pin and the centre of the follower locking pin, R_b the radius of the cam base circle and, finally, φ and δ_4 are constant values that are considered to be the angle between R_1 and R_2, and between R_4 and the imaginary horizontal axis that crosses the centre of the cam locking pin, respectively.

[12] The scale presented in Figure 3.7 represents the actual scale read when taking the system's measurements and not the scale that can be seen in this document.

[13] Since the photograph was not exactly centred, the actual centroid of the pin face is deviated, as shown in Figure 3.7.

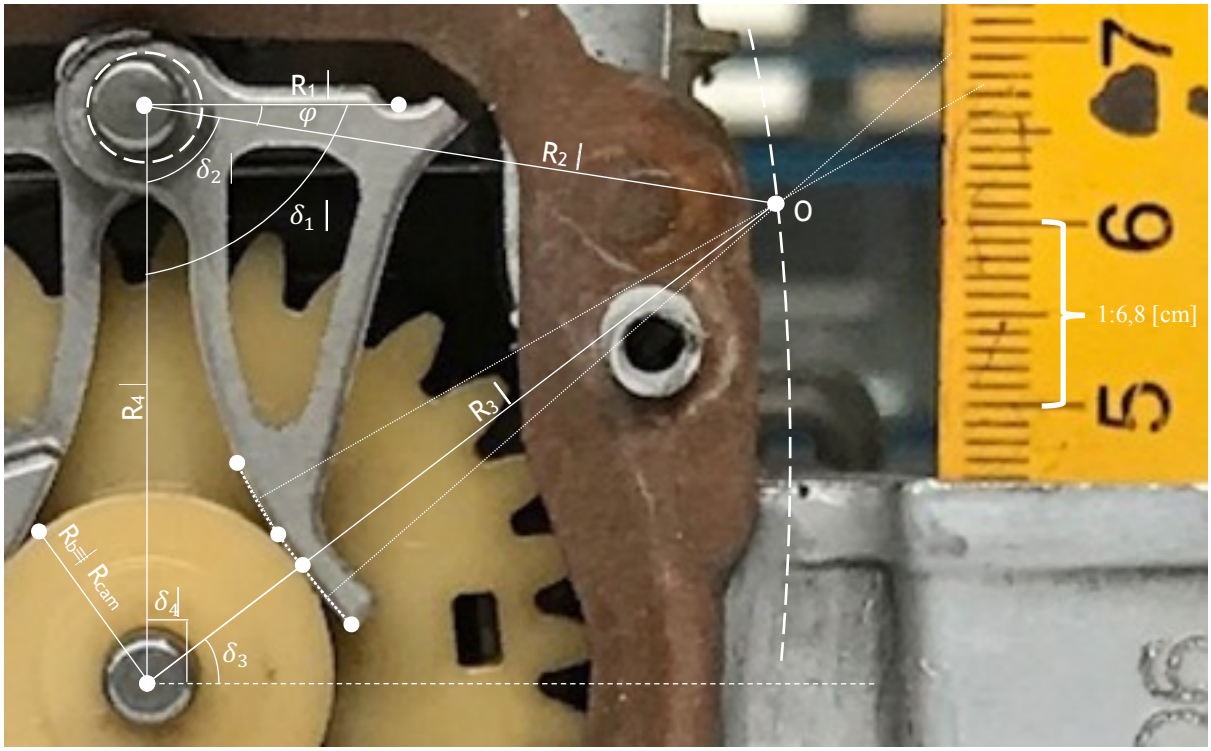

Figure 3.7 - Representative diagram of the different measurements made in order to dimension the cam profile.

The measured values are as follows:

$$R_1 = \frac{93{,}8}{6{,}8} = 13.8\ \text{mm}$$

$$R_2 = \frac{240}{6{,}8} = 35.3\ \text{mm}$$

$$R_4 = \frac{206{,}7}{6{,}8} = 30.4\ \text{mm}$$

$$R_b = 10\ \text{mm}$$

$$\varphi = 8.7°$$

$$\delta_4 = 90°$$

Although the values shown above will be the basis of the design, there are still some unknown variables, starting with R_3 which was not specified as a fixed value like the rest of the measured distances. This is due to the fact that R_3 varies with the cam radius which, in the case of Figure 3.7 is equal to R_b, but when the cam rotates to other positions, will have different values because of the "nose" seen in Figure 3.4 (see Fig. C.1 of Appendix C), i.e. the enlarged photograph depicted in Figure 3.7, allowed for the measurement of one R_3 value, which is:

$$R_3 = \frac{226}{6.8} + 10 = 43.2\ \text{mm}$$

which is an approximated value and, for this reason, further ahead an equation to solve for all the values of R_3 is deducted and those are the values used when designing the cam.

Having said this, and before mentioning the rest of the variables shown in Figure 3.7, such as δ_1, δ_2 and δ_3, it is very important to understand the logic behind the dimensioning presented in this section. What is happening is that it is being considered that the whole system represented in Figure 3.7 rotates around the cam, following the represented dashed trajectory passing through point O, with the result being that this trajectory, once a full cycle is completed, will represent an enlarged version of the actual cam profile, which will afterwards be reduced to its' actual size. To achieve this, there are three variables that have to be used, besides the ones that were already mentioned, and they are δ_1, δ_2 and δ_3, which represent different angles that vary throughout the entire cycle. They are intricately related to the remainder of the mentioned variables and constants, as follows:

$$\delta_1 = \frac{s}{R_1} \tag{3.5}$$

$$\delta_2 = \delta_1 - \varphi \tag{3.6}$$

with *s* being the follower displacement values from equation (3.1) for each angular position and, in order to simplify the next part, the value of δ_4 will be displayed in radians (instead of having $\delta_4 = 90°$, we shall have $\delta_4 = \frac{\pi}{2}$ rad):

$$\overrightarrow{R_3} = \overrightarrow{R_4} + \overrightarrow{R_2} \Leftrightarrow$$

$$\Leftrightarrow R_3 e^{i.\delta_3} = R_4 e^{i.\delta_4} + R_2 e^{i.\delta_2} \Longrightarrow$$

$$\overset{\delta_4=\frac{\pi}{2}}{\Longrightarrow} R_3 e^{i.\delta_3} = R_4 e^{i.\frac{\pi}{2}} + R_2 e^{i.\delta_2} \Leftrightarrow$$

$$\Leftrightarrow R_3 e^{i(\delta_3 - \frac{\pi}{2})} = R_4 e^{i.0} + R_2 e^{i(\delta_2 - \frac{\pi}{2})} \Leftrightarrow$$

Separating the real and imaginary parts into a system of equations:

$$\begin{cases} R_3 \cos\left(\delta_3 - \frac{\pi}{2}\right) = R_4 + R_2 \cos\left(\delta_2 - \frac{\pi}{2}\right) \\ R_3 \sin\left(\delta_3 - \frac{\pi}{2}\right) = R_2 \sin\left(\delta_2 - \frac{\pi}{2}\right) \end{cases} \Leftrightarrow \tag{3.7}$$

$$\Leftrightarrow \begin{cases} {R_3}^2 \cos^2\left(\delta_3 - \frac{\pi}{2}\right) = {R_4}^2 + 2R_4R_2 \cos\left(\delta_2 - \frac{\pi}{2}\right) + {R_2}^2 \cos^2\left(\delta_2 - \frac{\pi}{2}\right) \\ {R_3}^2 \sin^2\left(\delta_3 - \frac{\pi}{2}\right) = {R_2}^2 \sin^2\left(\delta_2 - \frac{\pi}{2}\right) \end{cases} \tag{3.8}$$

and afterwards adding the first and second equations, in system (3.8), term by term, it is possible to obtain:

$$R_3{}^2\left[\cos^2\left(\delta_3-\frac{\pi}{2}\right)+\sin^2\left(\delta_3-\frac{\pi}{2}\right)\right] = R_4{}^2+2R_4R_2\cos\left(\delta_2-\frac{\pi}{2}\right)+R_2{}^2\left[\cos^2\left(\delta_2-\frac{\pi}{2}\right)+\sin^2\left(\delta_2-\frac{\pi}{2}\right)\right]$$

Substituting the values according to the first Pythagorean identity of trigonometry:

$$R_3{}^2 = R_4{}^2+2R_4R_2\cos\left(\delta_2-\frac{\pi}{2}\right)+R_2{}^2 \Leftrightarrow$$

$$\Leftrightarrow R_3 = \sqrt{R_4{}^2+R_2{}^2+2R_4R_2\cos\left(\delta_2-\frac{\pi}{2}\right)} \quad (3.9)$$

which gives the general equation for R_3 and, by returning to the system of equations (3.7) and dividing the second equation by the first it is possible to obtain:

$$\frac{\cancel{R_3}\sin\left(\delta_3-\frac{\pi}{2}\right)}{\cancel{R_3}\cos\left(\delta_3-\frac{\pi}{2}\right)} = \frac{R_2\sin\left(\delta_2-\frac{\pi}{2}\right)}{R_4+R_2\cos\left(\delta_2-\frac{\pi}{2}\right)} \Leftrightarrow$$

$$\Leftrightarrow \tan\left(\delta_3-\frac{\pi}{2}\right) = \frac{R_2\sin\left(\delta_2-\frac{\pi}{2}\right)}{R_4+R_2\cos\left(\delta_2-\frac{\pi}{2}\right)} \Leftrightarrow$$

$$\Leftrightarrow \delta_3 = \tan^{-1}\left[\frac{R_2\sin\left(\delta_2-\frac{\pi}{2}\right)}{R_4+R_2\cos\left(\delta_2-\frac{\pi}{2}\right)}\right]+\frac{\pi}{2} \quad (3.10)$$

which gives, finally, the last needed equation to complete the objective of deducing all the constants and variables shown in Figure 3.7. It is important to note that, in this case, δ_3 will have the same values throughout the interval as the cam rotation angle, with the only difference being the point chosen to be the start of the profile design process.

After having deduced, in Section 3.2, the polynomial function that adapts to the behaviour of the measured valve lift and confirming that the fundamental law of cam design and its' corollary are met and afterwards, in this section, deduced all the variables and constants needed to design the cam profile, applying those conditions to the whole rotation of the cam was required, by means of the implemented model in the Microsoft Excel software that will, in turn, return the Cartesian coordinates of the different cam profile points. Since it was established that the values of δ_3 are

equal to the cA values and based on the diagram represented in Figure 3.7, the coordinates are deduced as follows:

$$X = R_3 \cos\left(\frac{\theta}{2}\right) \tag{3.11}$$

$$Y = R_3 \sin\left(\frac{\theta}{2}\right) \tag{3.12}$$

with θ being the CA[14].

By plotting the X and Y coordinates, as a smoothed curve scatter chart in the Microsoft Excel software, one gets the cam profiles according to the dimensions of R_3, as shown in Figure 3.8.

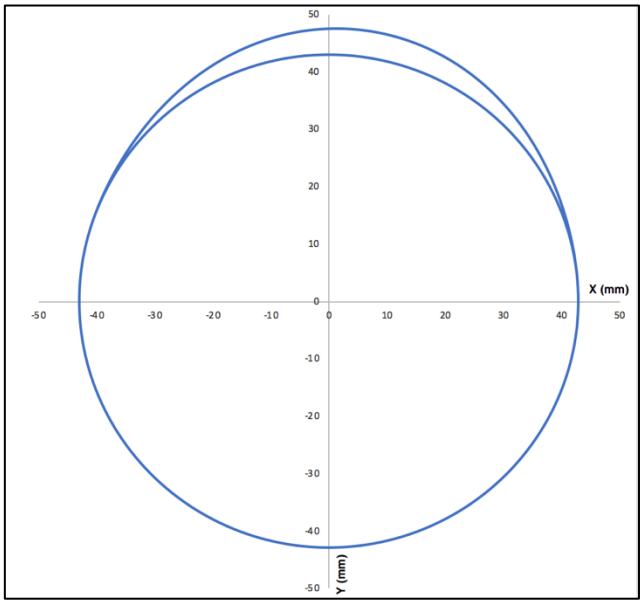

Figure 3.8 - Smoothed curve scatter plot of the cam profile points, according to R_3, the "outer cam profile"

The next step is to dimension the profile according to the cam radius and not to R_3. This can be achieved through a point translation process from the cam profile seen in Figure 3.8, in order to create the actual cam profile, with the dimensions of the Honda GX31 original cam. This process begins by focusing on one of the many points already plotted, A(X;Y), then also the neighbouring points of the first one (one before and one after), B(X;Y) and C(X;Y), and hypothesizing that a linear segment connects B(X,Y) and C(X,Y), creating segment $\overline{BC}$. Another linear segment, perpendicular to $\overline{BC}$ and containing point A(X;Y) is drawn, of which the length will be equal to R_3, giving us the position of the first point of the actual cam profile, A'(x_c;y_c), as shown in Figure 3.9.

[14] Due to the fact that the cam rotates at half the speed of the crankshaft, θ is divided by two.

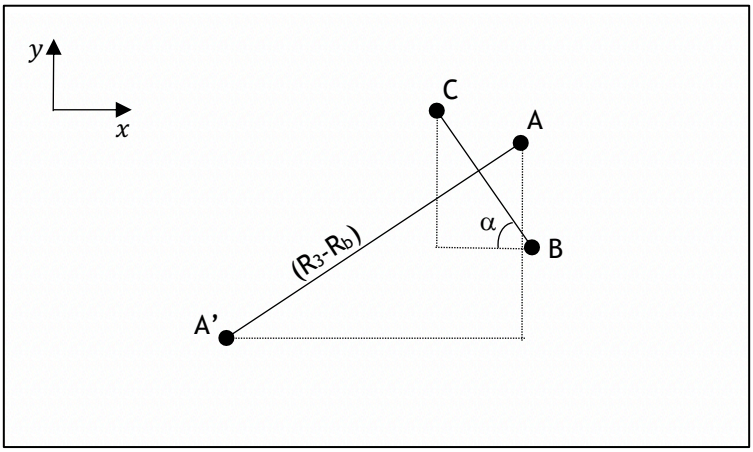

Figure 3.9 - Representative diagram of the described process of point translation to create the actual cam profile

Although Figure 3.9 is an exaggeration in terms of distances and angles, the principle is the same, in which we shall have to deduce a formula to solve for the abscissas and the ordinates, a formula that must contain parameters that are easy to manipulate and adjust to the desired requirements.

The first step is to deduce the expression for α, according to the coordinates of points B and C:

$$\tan(\alpha) = \frac{\mathrm{Y_C} - \mathrm{Y_B}}{\mathrm{X_C} - \mathrm{X_B}} \Leftrightarrow$$

$$\Leftrightarrow \alpha = \tan^{-1}\left(\frac{\mathrm{Y_C} - \mathrm{Y_B}}{\mathrm{X_C} - \mathrm{X_B}}\right)$$

Seeing as the distance between A and A' is equal to subtracting R_b to R_3, one simply has to find the relation between the coordinates of both points:

$$(X_A - x_{c_A}) = \cos\left(\alpha + \frac{\pi}{2}\right).(R_3 - R_b) \Leftrightarrow$$

$$\Leftrightarrow x_{c_{A'}} = X_A + (R_3 - R_b).\cos\left[\tan^{-1}\left(\frac{\mathrm{Y_C} - \mathrm{Y_B}}{\mathrm{X_C} - \mathrm{X_B}}\right) + \frac{\pi}{2}\right]$$

in which, $\mathrm{x_{c_{A'}}}$ is the abscissa of point A' and $\left(\alpha + \frac{\pi}{2}\right)$ is used in order for the direction of the translation to be perpendicular to $\overline{\mathrm{BC}}$. Similarly, for the ordinates:

$$(Y_A - y_{c_A}) = \sin\left(\alpha + \frac{\pi}{2}\right).(R_3 - R_b) \Leftrightarrow$$

$$\Leftrightarrow y_{c_{A'}} = Y_A + (R_3 - R_b).\sin\left[\tan^{-1}\left(\frac{\mathrm{Y_C} - \mathrm{Y_B}}{\mathrm{X_C} - \mathrm{X_B}}\right) + \frac{\pi}{2}\right]$$

in which, $y_{c_{A'}}$ is the ordinate of point A' and $\left(\alpha+\frac{\pi}{2}\right)$ is used in order for the direction of the translation to be perpendicular to $\overline{BC}$. However, since the final result will have to be present in all four quadrants of the Cartesian plot, some conditions have to be met in order for the result to be accurate. Those conditions are as follows:

$$x_c = \begin{cases} X_A + (R_3 - R_b) * \cos\left[\tan^{-1}\left(\frac{Y_C - Y_B}{X_C - X_B}\right) + \frac{\pi}{2}\right], & X_c - X_B < 0 \\ X_A - (R_3 - R_b) * \cos\left[\tan^{-1}\left(\frac{Y_C - Y_B}{X_C - X_B}\right) + \frac{\pi}{2}\right], & X_c - X_B \geq 0 \end{cases} \quad (3.13)$$

$$y_c = \begin{cases} Y_A + (R_3 - R_b) * \sin\left[\tan^{-1}\left(\frac{Y_C - Y_B}{X_C - X_B}\right) + \frac{\pi}{2}\right], & X_c - X_B < 0 \\ Y_A - (R_3 - R_b) * \sin\left[\tan^{-1}\left(\frac{Y_C - Y_B}{X_C - X_B}\right) + \frac{\pi}{2}\right], & X_c - X_B \geq 0 \end{cases} \quad (3.14)$$

The process is then iterated for every single point contained in the "outer cam profile" thus returning the actual cam profile, and in order to do this, an IF function will have to be applied to the Microsoft Excel formula, due to the two different conditions presented both in system (3.13) and (3.14). Once all the cells have been formatted to give the new coordinates for the cam profile, the following result is obtained, with the blue curve being the same presented in Figure 3.9, and the black one being the actual cam profile of the Honda GX31 cam (see Fig. 3.10).

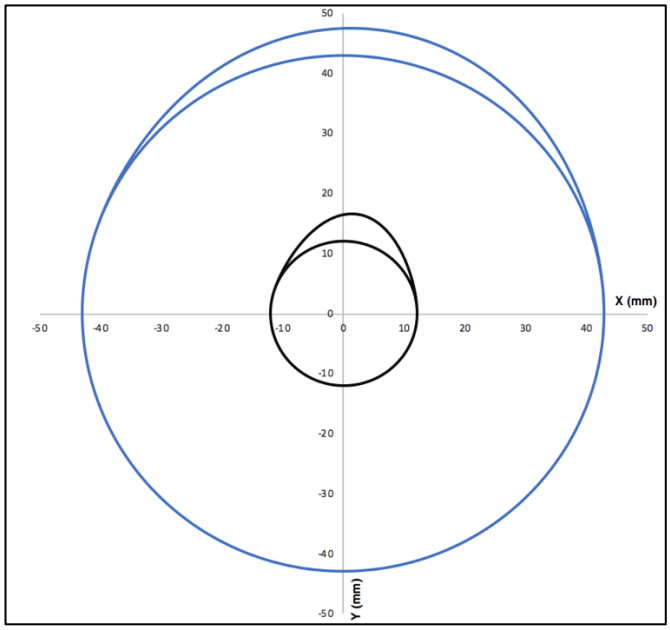

Figure 3.10 - "Outer cam profile" in blue and the actual Honda GX31 cam profile in black.

Having created a worksheet in the Microsoft Excel software that allows for the creation of different cam profiles, based on the valve duration, lift and opening point, the next step is to understand what alterations will have to be made to the cam profile, in order for the Honda GX31 engine to perform better at lower engine speeds, which will be discussed in the next section.

3.4 New cam profile

3.4.1 First design attempt

In the last section was mentioned the creation process of the cam profile generation, which will be fundamental in order to find a new cam profile and attempt to manufacture it afterwards. As it has been said before, the main objective of this experiment is to alter the Honda GX31 cam in order to improve its' performance at lower engine speeds, due to the fact that it is a very high-revving engine (about 3000 rpm idle to about 8500 rpm at WOT) and in order to attempt to use it as a means of propulsion for a small UAV, it has to perform equally well at lower engine speeds.

From the literature, it can be concluded that reducing valve duration and overlap (to about 250º or less of duration and 50º or less of overlap), in high-speed cam-follower systems, can broaden the engines' usable power band and also make it possible for this power band to "shift" to lower engine speed intervals (from about 3000-8000 rpm to about 2000-7500 rpm). It is with this knowledge that a new cam profile design will be attempted, through the Microsoft Excel software. The Microsoft Excel spreadsheet mentioned in Section 3.3 was designed and built with the formulas containing variables, i.e. instead of using actual values, cell references that could be altered at will were used, and altering those values will alter the entire finished cam profile, making the process much quicker.

Having said this, the first design was attempted by simply changing the duration from 330º to 250º, which produced a very sharp-pointed cam profile (see Fig. D.1 of Appendix D), which would be very prejudicial and unreliable due to the extreme stresses that would be transmitted to the cam-follower system if the design was kept like that. The logical way around this was to reduce the amount of lift (from 2.7 mm to 2.5 mm) and widen the R_b of the cam (from 10 mm to 12 mm), resulting in a much smoother cam profile (see Fig. D.2 of Appendix D) that could, after a structural analysis of the contact stresses between the cam and the follower was made, be suitable for manufacturing by exporting the profile to the CATIAV5 software, designing the spur gear and sending the result to the UBI machine shop (called the FABLAB) for fabrication in aluminium through means of a milling cutter.

Unfortunately, due to the lack of time and resources, a viable fabrication of this component in the desired amount of time was proven to be impossible, and another alternative had to be pursued.

3.4.2 Aluminium cam lift measurement

Despite not being possible to go through to the end with the first design attempt, an alternative was found that could allow for the experimental procedure.

Thanks to the combined efforts of the DCA and the Department of Electromechanical Engineering (or DEM), an aluminium cam that had been manufactured years before to be implemented in a Honda GX31 to use as a propulsion system for the UBI's Shell Eco-marathon vehicle was acquired for this experimental study and found to have had nearly the same design characteristics as the ones that were aimed for with this study. Even though the end goal was not the same, for in the case of the Shell Eco-marathon, the main objective was to reduce the SFC and boost the range of the vehicle in question, the means to get to that end derived from the same logic that was mentioned earlier, which was to reduce the valve duration and overlap, in order for the engine to be able to function well at slower engine speeds.

However, there was a disadvantage to this alternative, which was the fact that no information could be found about the specifications of the cam itself, aside from the design logic mentioned above and whatever physical measurements made afterwards. What this meant, was that a whole new study about this particular cam had to be made, like the one made for the original cam in the Honda GX31, in order to fully understand the specifications of the new cam. For this, the valve lift measurement procedure detailed in Section 3.1 was repeated with the new cam installed, giving the results shown in Fig. 3.11.

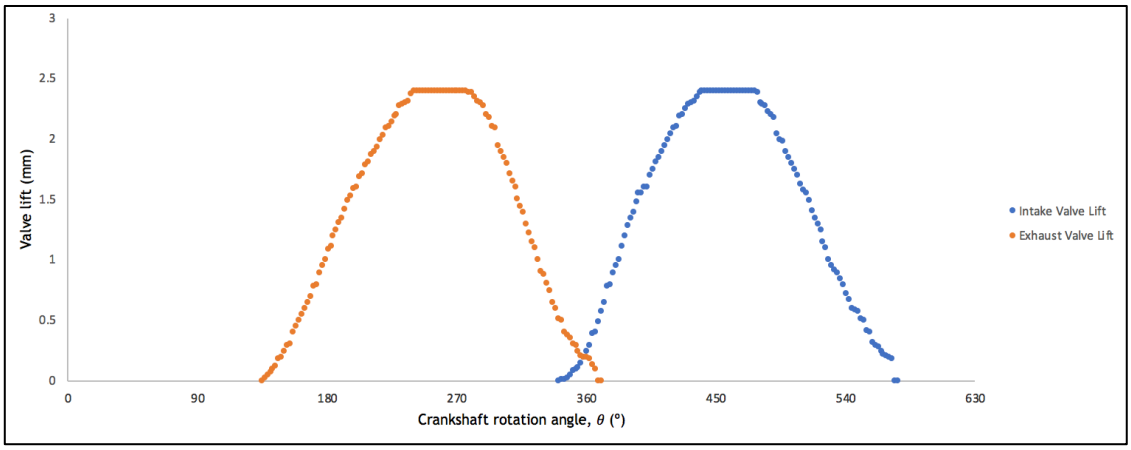

Figure 3.11 – Scatter point chart made with the Microsoft Excel software, depicting the valve lift measurements made to the new aluminium cam.

Since the apparatus was built with the same equipment as before, all the sources for measurement imprecisions mentioned in Section 3.1, with the exception that the new cam did not have a compression release mechanism, were present and, with these measurements, came the specifications presented in Table 4.1.

Table 4.1 - New cam measured specifications, with the angle values expressed in CA.

IVO (°)	338
IVC(°)	574
EVO(°)	138
EVC(°)	374

Valve Duration (°)	236
Valve Overlap (°)	36
Valve Gap at Maximum Lift (°)	200
Maximum Lift (mm)	2.4

From Table 4.1 it is possible to conclude that the duration and overlap benchmarks of 250° and 50° respectively, mentioned in the previous section, were not only met but surpassed, as well as the benchmark maximum lift value of 2.5 mm. These are very positive starting points to the new cam design study, from the perspective of accomplishing the main objectives.

3.4.3 Aluminium cam motion equations and s-v-a-j diagram

As it was done before for the original cam, a polynomial motion function will be deduced for the new aluminium cam, starting with a sixth-degree polynomial with same BCs as mentioned in Section 3.2, the new values of L and β can be substituted in equations (2.18-2.21) to get:

$$s = 2{,}4\left[64\left(\frac{\theta}{236}\right)^3 - 192\left(\frac{\theta}{236}\right)^4 + 192\left(\frac{\theta}{236}\right)^5 - 64\left(\frac{\theta}{236}\right)^6\right] \tag{3.15}$$

$$v = \frac{2{,}4}{236}\left[192\left(\frac{\theta}{236}\right)^2 - 768\left(\frac{\theta}{236}\right)^3 + 960\left(\frac{\theta}{236}\right)^4 - 384\left(\frac{\theta}{236}\right)^5\right] \tag{3.16}$$

$$a = \frac{2{,}4}{236^2}\left[384\left(\frac{\theta}{236}\right) - 2304\left(\frac{\theta}{236}\right)^2 + 3840\left(\frac{\theta}{236}\right)^3 - 1920\left(\frac{\theta}{236}\right)^4\right] \tag{3.17}$$

$$j = \frac{2{,}4}{236^3}\left[384 - 4608\left(\frac{\theta}{236}\right) + 11520\left(\frac{\theta}{236}\right)^2 - 7680\left(\frac{\theta}{236}\right)^3\right] \tag{3.18}$$

and, to check if this polynomial function adapts to the measured one, the displacement polynomial curve was plotted alongside the measured one (see Fig. 3.12).

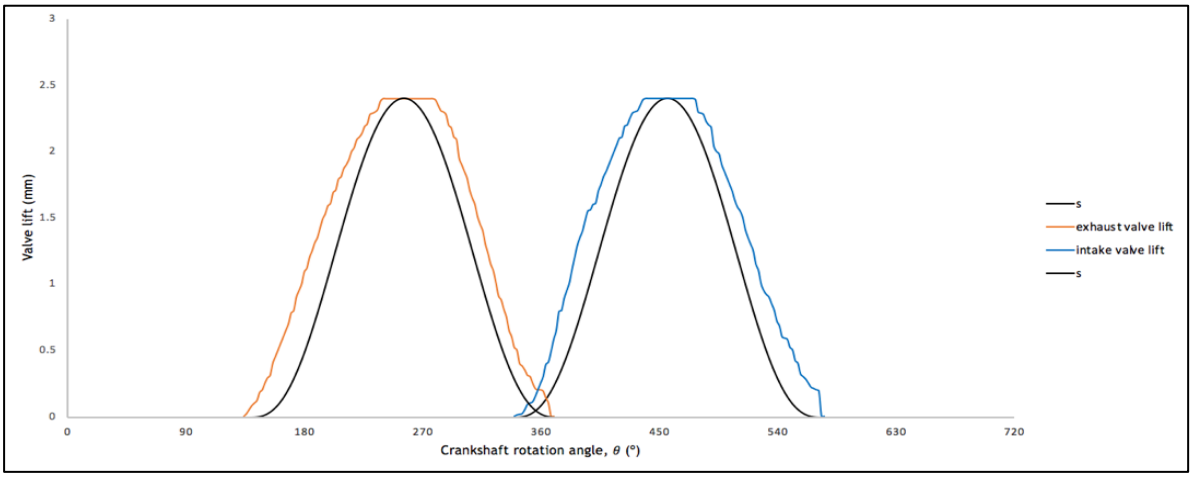

Figure 3.12 - The sixth-degree polynomial alongside the lift measurements.

which, as it can be seen, does not adapt to the measured lift of this particular cam, meaning that adding more BCs will be needed in order to get the polynomial displacement function to correctly adapt to the measured one.

From Figure 3.12, it is seen that the sixth-degree polynomial does not rise, nor fall fast enough to adapt correctly to the measured lift values, which is why there is a need to add other BCs to the already existing ones. Starting with a point at $\beta/4$ which, from the measurements, is known to happen 59º after the opening of either of the valves and has a lift of 1,58 mm. However, this condition alone does not suffice, due to the fact that by adding this BC, the polynomial function would not assume the 2.4 mm mark as its' maximum lift point, and therefore, for this to happen, another constraint has to be added, which is that the velocity must be zero at $\beta/2$. With this last BC added, the polynomial function now "knows" that at 2.4 mm of displacement, the first derivative has to be zero and, consequently, the displacement curve has to have a dwell through those values. The new set of BCs, then, is presented in Table 4.2.

Table 4.2 - Boundary conditions in order to obtain a 5-6-7-8 polynomial function.

Position of θ according to β	Boundary Conditions		
θ = 0	s=0	v=0	a=0
θ = β/4	$s=L_{1/4}$		
θ = β/2	s=L	v=0	
θ = β	s=0	v=0	a=0

with $L_{1/4}$ being the valve lift at ¼ of the duration and L being the maximum valve lift.

By looking at Table 4.2, it can be concluded that, by having 9 BCs, according to equation (2.6), an eight-degree polynomial will be generated to accommodate these BCs. Deriving the correct eighth-degree polynomial follows the same procedure shown in Section 3.1, but instead of having 6 BCs, 8 are present, which means that equations (2.7-2.10) become:

$$s = C_0 + C_1\left(\frac{\theta}{\beta}\right) + C_2\left(\frac{\theta}{\beta}\right)^2 + C_3\left(\frac{\theta}{\beta}\right)^3 + C_4\left(\frac{\theta}{\beta}\right)^4 + C_5\left(\frac{\theta}{\beta}\right)^5 + C_6\left(\frac{\theta}{\beta}\right)^6 + C_7\left(\frac{\theta}{\beta}\right)^7 + C_8\left(\frac{\theta}{\beta}\right)^8 \quad (3.19)$$

$$v = \frac{1}{\beta}\left[C_1 + 2C_2\left(\frac{\theta}{\beta}\right) + 3C_3\left(\frac{\theta}{\beta}\right)^2 + 4C_4\left(\frac{\theta}{\beta}\right)^3 + 5C_5\left(\frac{\theta}{\beta}\right)^4 + 6C_6\left(\frac{\theta}{\beta}\right)^5 + 7C_7\left(\frac{\theta}{\beta}\right)^6 + 8C_8\left(\frac{\theta}{\beta}\right)^8\right] \quad (3.20)$$

$$a = \frac{1}{\beta^2}\left[2C_2 + 6C_3\left(\frac{\theta}{\beta}\right) + 12C_4\left(\frac{\theta}{\beta}\right)^2 + 20C_5\left(\frac{\theta}{\beta}\right)^3 + 30C_6\left(\frac{\theta}{\beta}\right)^4 + 42C_7\left(\frac{\theta}{\beta}\right)^5 + 64C_8\left(\frac{\theta}{\beta}\right)^6\right] \quad (3.21)$$

$$j = \frac{1}{\beta^3}\left[6C_3 + 24C_4\left(\frac{\theta}{\beta}\right) + 60C_5\left(\frac{\theta}{\beta}\right)^2 + 120C_6\left(\frac{\theta}{\beta}\right)^3 + 210C_7\left(\frac{\theta}{\beta}\right)^4 + 384C_6\left(\frac{\theta}{\beta}\right)^5\right] \quad (3.22)$$

From there and following the same procedure used in Section 2.6.3, it is clear that, despite having more BCs this time around, the first three constant coefficients are the same:

$$\begin{cases} C_0 = 0 \\ C_1 = 0 \\ C_2 = 0 \end{cases}$$

and the differences only start appearing when solving for the last 6 constant coefficients. Substituting the following BCs:

θ = β/2	s=L	v=0

in equations (3.19-3.20), it is possible to obtain:

$$L = C_3\frac{1}{8} + C_4\frac{1}{16} + C_5\frac{1}{32} + C_6\frac{1}{64} + C_7\frac{1}{128} + C_8\frac{1}{256} \quad (3.23)$$

and:

$$0 = \frac{1}{\beta}\left[3C_3\left(\frac{1}{4}\right) + 4C_4\left(\frac{1}{8}\right) + 5C_5\left(\frac{1}{16}\right) + 6C_6\left(\frac{1}{32}\right) + 7C_7\left(\frac{1}{64}\right) + 8C_8\left(\frac{1}{128}\right)\right] \quad (3.24)$$

Afterwards, by substituting:

θ = β	s=0	v=0	a=0

In equations (3.19-3.21) it is possible to obtain:

$$C_3 + C_4 + C_5 + C_6 + C_7 + C_8 = 0 \quad (3.25)$$

$$\frac{1}{\beta}(3C_3 + 4C_4 + 5C_5 + 6C_6 + 7C_7 + 8C_8) = 0 \tag{3.26}$$

and:

$$\Leftrightarrow \frac{1}{\beta^2}[6C_3 + 12C_4 + 20C_5 + 30C_6 + 42C_7 + 56C_8] = 0 \tag{3.27}$$

Finally, to get the last equation needed to simultaneously solve all the constant coefficients, is substituted:

θ = β/4	$s=L_{1/4}$

in equation (3.19), to get:

$$\Leftrightarrow L_{1/4} = C_3\frac{1}{64} + C_4\frac{1}{256} + C_5\frac{1}{1024} + C_6\frac{1}{4096} + C_7\frac{1}{16384} + C_8\frac{1}{65536} \tag{3.28}$$

Which means that now there are 6 equations to solve for 6 constant coefficients, as was done before, in Section 2.6.3. Joining equations (3.23-3.28) in a matrix system:

$$\begin{bmatrix} \frac{1}{8} & \frac{1}{16} & \frac{1}{32} & \frac{1}{64} & \frac{1}{128} & \frac{1}{256} \\ \frac{1}{64} & \frac{1}{256} & \frac{1}{1024} & \frac{1}{4096} & \frac{1}{16384} & \frac{1}{65536} \\ \frac{3}{4}x & \frac{1}{2}x & \frac{5}{16}x & \frac{3}{16}x & \frac{7}{64}x & \frac{1}{16}x \\ 1 & 1 & 1 & 1 & 1 & 1 \\ 3x & 4x & 5x & 6x & 7x & 8x \\ 6x^2 & 12x^2 & 20x^2 & 30x^2 & 42x^2 & 56x^2 \end{bmatrix} \begin{bmatrix} C_3 \\ C_4 \\ C_5 \\ C_6 \\ C_7 \\ C_8 \end{bmatrix} = \begin{bmatrix} L \\ L_{1/4} \\ 0 \\ 0 \\ 0 \\ 0 \end{bmatrix}, \text{with } x = \frac{1}{\beta}$$

$$\begin{cases} C_3 = \dfrac{16384L_{1/4} - 5184L}{27} \\ C_4 = -\dfrac{114688L_{1/4} + 43200L}{27} \\ C_5 = \dfrac{311296L_{1/4} - 126144L}{27} \\ C_6 = -\dfrac{409600L_{1/4} + 171072L}{27} \\ C_7 = \dfrac{262144L_{1/4} - 110592L}{27} \\ C_8 = -\dfrac{65536L_{1/4} + 27648L}{27} \end{cases}, \text{with } \beta \neq 0 \tag{3.29}$$

Meaning that the complete s-v-a-j equations are:

$$\begin{aligned} s = {} & \left(\frac{16384L_{1/4} - 5184L}{27}\right)\left(\frac{\theta}{\beta}\right)^3 + \left(-\frac{114688L_{1/4} + 43200L}{27}\right)\left(\frac{\theta}{\beta}\right)^4 \\ & + \left(\frac{311296L_{1/4} - 126144L}{27}\right)\left(\frac{\theta}{\beta}\right)^5 + \left(-\frac{409600L_{1/4} + 171072L}{27}\right)\left(\frac{\theta}{\beta}\right)^6 \\ & + \left(\frac{262144L_{1/4} - 110592L}{27}\right)\left(\frac{\theta}{\beta}\right)^7 + \left(-\frac{65536L_{1/4} + 27648L}{27}\right)\left(\frac{\theta}{\beta}\right)^8 \end{aligned} \tag{3.30}$$

$$\begin{aligned} v = {} & \frac{1}{\beta}\left[3\left(\frac{16384L_{\frac{1}{4}} - 5184L}{27}\right)\left(\frac{\theta}{\beta}\right)^2 + 4\left(-\frac{114688L_{1/4} + 43200L}{27}\right)\left(\frac{\theta}{\beta}\right)^3\right. \\ & + 5\left(\frac{311296L_{1/4} - 126144L}{27}\right)\left(\frac{\theta}{\beta}\right)^4 + 6\left(-\frac{409600L_{1/4} + 171072L}{27}\right)\left(\frac{\theta}{\beta}\right)^5 \\ & \left. + 7\left(\frac{262144L_{1/4} - 110592L}{27}\right)\left(\frac{\theta}{\beta}\right)^6 + 8\left(-\frac{65536L_{1/4} + 27648L}{27}\right)\left(\frac{\theta}{\beta}\right)^8\right] \end{aligned} \tag{3.31}$$

$$\begin{aligned} a = {} & \frac{1}{\beta^2}\left[6\left(\frac{16384L_{1/4} - 5184L}{27}\right)\left(\frac{\theta}{\beta}\right) + 12\left(-\frac{114688L_{1/4} + 43200L}{27}\right)\left(\frac{\theta}{\beta}\right)^2\right. \\ & + 20\left(\frac{311296L_{1/4} - 126144L}{27}\right)\left(\frac{\theta}{\beta}\right)^3 \\ & + 30\left(-\frac{409600L_{1/4} + 171072L}{27}\right)\left(\frac{\theta}{\beta}\right)^4 \\ & \left. + 42\left(\frac{262144L_{1/4} - 110592L}{27}\right)\left(\frac{\theta}{\beta}\right)^5 + 64\left(-\frac{65536L_{1/4} + 27648L}{27}\right)\left(\frac{\theta}{\beta}\right)^6\right] \end{aligned} \tag{3.32}$$

$$\begin{aligned} j = {} & \frac{1}{\beta^3}\left[6\left(\frac{16384L_{1/4} - 5184L}{27}\right) + 24\left(-\frac{114688L_{1/4} + 43200L}{27}\right)\left(\frac{\theta}{\beta}\right)\right. \\ & + 60\left(\frac{311296L_{1/4} - 126144L}{27}\right)\left(\frac{\theta}{\beta}\right)^2 \\ & + 120\left(-\frac{409600L_{1/4} + 171072L}{27}\right)\left(\frac{\theta}{\beta}\right)^3 \\ & + 210\left(\frac{262144L_{1/4} - 110592L}{27}\right)\left(\frac{\theta}{\beta}\right)^4 \\ & \left. + 384\left(-\frac{65536L_{1/4} + 27648L}{27}\right)\left(\frac{\theta}{\beta}\right)^5\right] \end{aligned} \tag{3.33}$$

Herein lies proof of what was mentioned in Section 2.6.3 about higher degree polynomials being much more complex than lower degree ones. Verification of the displacement motion function adaptation to the measured valve lift curves is presented in Fig. 3.13.

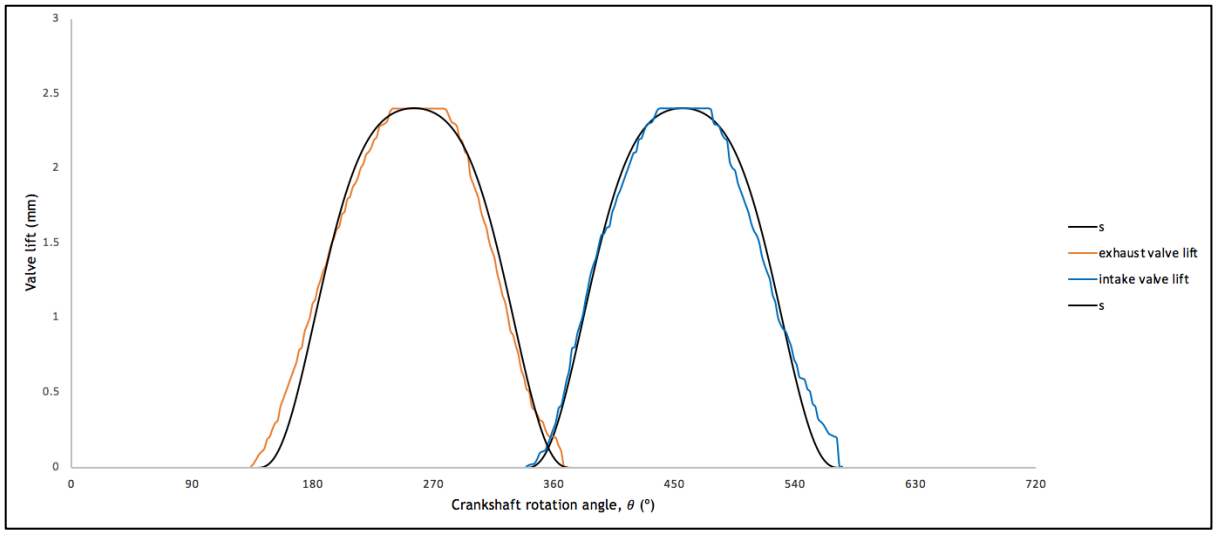

Figure 3.13 – Smoothed curve scatter plot of the eight-degree polynomial curves alongside the measured valve lift curves.

As it is possible to conclude from Figure 3.13, the derived polynomial function adapts accurately to the valve lift measurement curves, which means the last verification that needs to be done is to check that the motion function complies with the fundamental law of cam design and its' corollary, mentioned in Section 2.6, by plotting the s-v-a-j diagram (see Fig. 3.14).

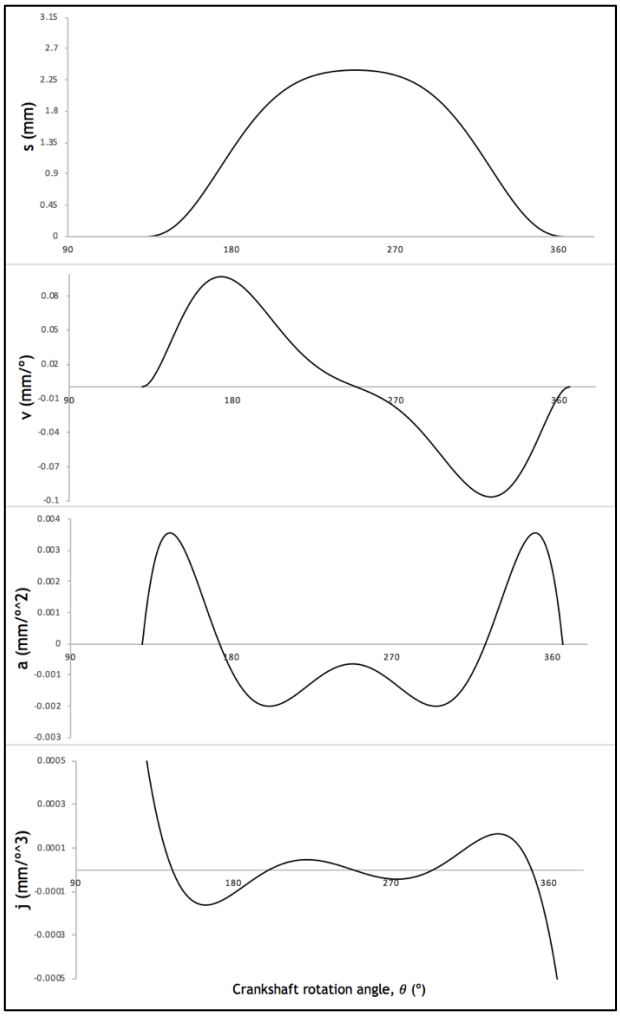

Figure 3.14 - Smoothed curve scatter plot of the 5-6-7-8 polynomial s-v-a-j diagram according to equations (3.30-3.33).

Having plotted the complete s-v-a-j diagram, it can be confirmed that the first and second derivatives are continuous throughout the entire measured interval and that the third derivative is finite throughout the same interval. This leads to the conclusion that this particular motion function can accurately describe the aluminium cam behaviour throughout the entire CA interval.

Finally, and despite not being relevant to the results, in Figure 3.14, the resulting cam profile, from the Microsoft Excel spreadsheet that was created, is presented and, straightway, it is possible to visualize that this cam profile is not exactly equal to the actual aluminium cam shown in Appendix E. There are some reasons that can have caused this to happen, with the main one being the fact that the valve lift measurements probably contain some precision errors, which may have led to less accurate results than expected and caused the cam profile to slightly deviate from the expected result.

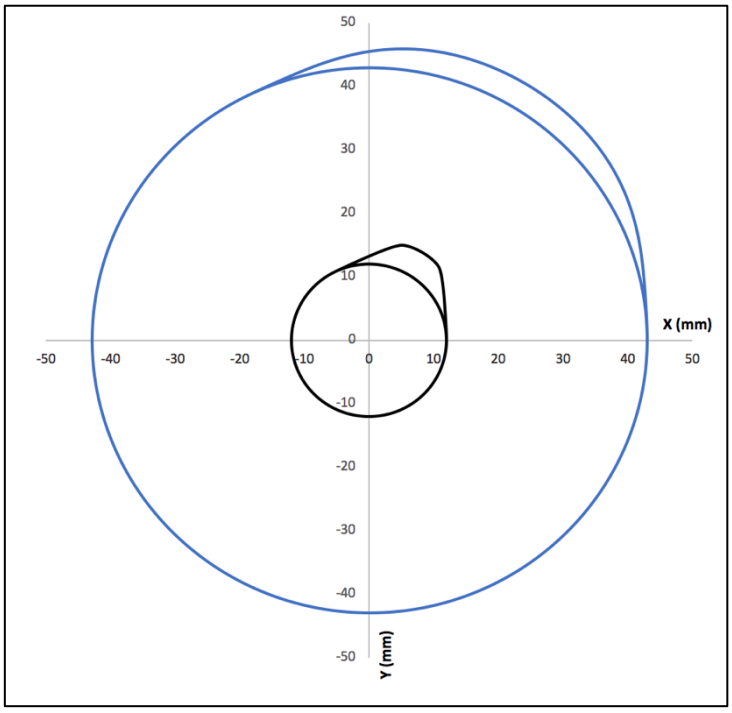

Figure 3.15 - Resulting cam profile from the implemented model.

Having studied the aluminium cam specifications, the next step would be to make a structural analysis based on the contact stresses between two cylindrical bodies, in order to make sure that the stress applied on the cam-follower system, more specifically on the actual follower, is not high enough to cause lasting damage.

When two cylindrical bodies subject to exterior loads come into contact with one another, as is the case of the Honda GX31 cam-follower system, contact stresses appear, as described in Figure 3.15, and studying this phenomenon becomes crucial when analysing the system. The Hertz theory is behind the solution for this type of mechanical problems, but for the sake of interest and space, the deduction will not be presented here, only the practical case that will allow the resolution of this specific case [15].

With basis on Figure 3.15, the contact stress deformation caused by two cylindrical bodies in contact, subject to an outside force, F, in the contact zone, has the length, l, of the cylinders themselves, with the width being [15]:

$$w = 2{,}15\left[\frac{F.d_1d_2}{E.l.(d_1+d_2)}\right]^{1/2} \tag{3.34}$$

where E is the elasticity module of the aluminium since it is the material from which both the new cam and the original follower are made of, l=7 mm, and d_1 and d_2 are the actual curvature diameters of the follower and cam, respectively. Having said this, the maximum contact stress for each curvature point is given by [15]:

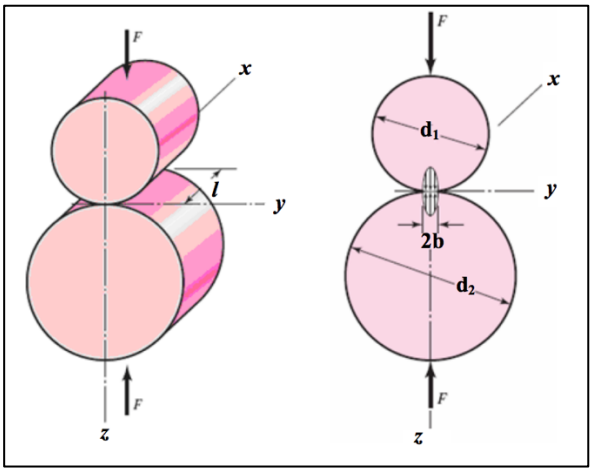

Figure 3.16 - Contact stresses of two cylindrical bodies subjected to outside forces [16].

$$\sigma_{max} = 0{,}59.\left[\frac{PE(d_1 + d_2)}{l d_1 d_2}\right] \tag{3.35}$$

In which F would be solved by using Newton's Second law of motion, $F = m.a$, with *m* being the mass of the full system, from cam to valve, and *a* being the acceleration of the system, which would mean having to disassemble the engine again, weigh every single part included, make a study of the valve spring forces, and of the inertia of the rocker arm, through 3D digitalization and analysis of the component with the adequate software.

However, since for this case, the cam was already manufactured, and in order to save time and space, this study was not made, despite it being very important and, should any other study be pursued, the structural analysis will have to be made in future work.

Chapter 4

Results and Discussion

4.1 Experiment components description

Like any other experimental project, there is a need to use a physical apparatus in order to log usable data to compare. In this chapter, a detailed description of the data logging system and mechanical measuring apparatus will be given and, afterwards, the results will be displayed and discussed in order to verify if the dissertation objectives were, or not, met.

4.1.1 Engine and propeller

Although the Honda GX31 specifications table has been mentioned before (see Table A.1 of Appendix A), it is also important to explain some of the operating characteristics of the engine. Despite not being a modern engine (appearing in 1997 and having been later replaced with Honda GX-35), the Honda GX31 is still used nowadays for a wide variety of applications that differ from the original aim of being incorporated in lawn and garden small equipment, including RC airplanes, cars and more [17]. Its' popularity derives from the durability, easy maintenance, compactness and power to weight ratio it presents, being one of the smallest four-stroke ICEs in the world, and also the possibility of working smoothly in any positional orientation desired.

In its' original disposition, the Honda GX31 has a recoil starter, which consists of a piece of string or rope that is attached to a pulley, which is, in turn, attached to the engine flywheel. When the operator pulls on the rope, the engine flywheel rotates and activates the engine magneto ignition system. This type of system has its' own electric generation that provides the necessary energy for the ignition to happen, through the presence of two magnets in the flywheel which, when rotated, create an electrical current on the primary windings of the ignition coil, which is then multiplied when transferred to the secondary windings, creating a spark at a much higher voltage than was originally received [18]. The coil's armature also contains a metal pin used to discharge the coil and stop the engine.

To make sure that the engine does not function load-free, and given the aeronautical interest behind this dissertation, a small propeller was chosen according to the performance specifications of the Honda GX31 and, after being acquired by the DCA, was installed on the engine in order to add a load

factor which is approximately constant throughout the entire engine speed interval, due to the fact that the test runs will be in a static environment and the propulsive efficiency of the propeller is approximately zero [19]. In this case, the propeller will work in the same way that the inertia wheel works in a regular test stand (explained in further detailed in Section 4.1.3), with the added bonus of being much lighter, helping with the cooling of the engine and, as mentioned before, being relevant to the aeronautical component behind the work being done.

Choosing the right propeller to install in an ICE or any other propulsion system is a process that involves two steps: understanding the historic use of a certain type of propeller for a certain type of propulsion system and confirming the first step through appropriate software. For small, piston engine UAVs with similar power bands to the Honda GX31, the most usual propeller size chosen is 17x10 (diameter of 17 in and pitch of 10 in), which can be confirmed through the PropSelector software, that consists of an extensive propeller database used to evaluate the users' input of different engine specifications and, with this information, predict the behaviour of the system throughout different flight conditions and choose the most appropriate propeller size to avoid overstressing the propeller or the engine. To sum up, and given the latter information, the propeller chosen was a wooden, 17x10 propeller [19].

4.1.2 Data logging system

In order to get and discuss results, a data logging system had to be employed into the experiment and, although there is a wide variety of systems, for this experiment an "Arduino and load cell" configuration was chosen to measure the engines' torque. Arduino is an open-source electronics platform, with user-friendly hardware, like the Arduino boards, and software, like the Arduino software (IDE); in which the Arduino boards are able to read a particular input (like a light on a sensor) and turning it into an output (like turning on an LED), according to the instructions given by the user through the programming language (an adaptation of C/C++) on the IDE software to the microcontroller on the actual board [20].

When it comes to the load cell, it is a piece of equipment that converts force into readable electrical outputs, through many different methods but, in this work, a bending beam load cell designed for a maximum of 5 kg was chosen, which is an aluminium bar, comprised of two or more resistances, that bends[15] when force is applied, creating a measurable differential on the resistances. It also contains four wires that connect to an outside micro amplifier (in this project, an HX711 board is used) used to amplify the electrical signal that is, then, sent to the Arduino board (in this project, an Arduino Nano is used) as it is possible to observe in Figure 4.1, in which the red wire connects to the E+ pin, the black wire to the E- pin, the white wire to the A- pin, the green wire to connects to the A+ and, from the HX711 board to the Arduino Nano board, the ground (GND) pin connects to the GND pin, the

[15] Since it is a solid aluminum bar, the flexing is not visible but it does happen.

dout (DT) pin connects to the D3 pin, the SCK pin connects to the D2 pin and, finally, the VCC pin connects to the 5V pin.

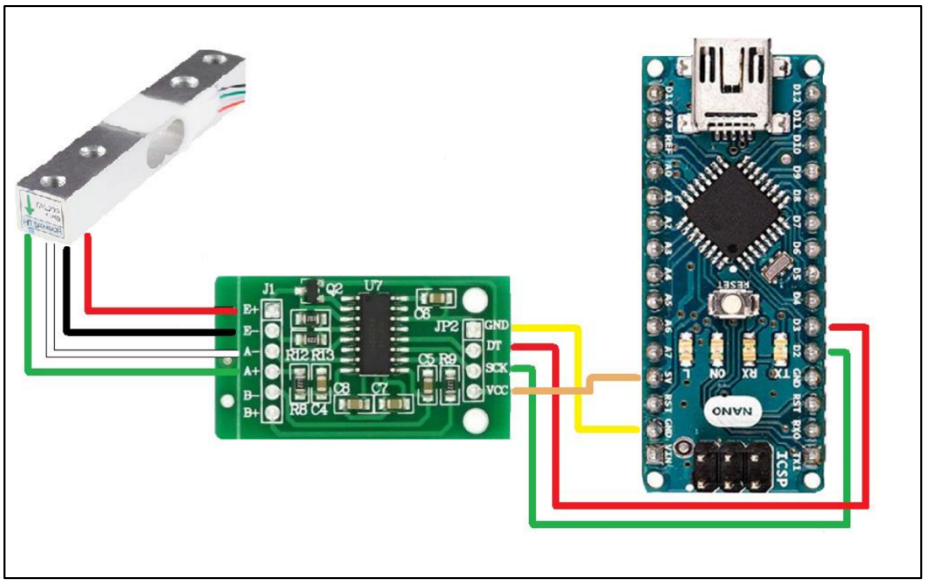

Figure 4.1 - Representative diagram of the connections made from the load cell to the Arduino Nano board [19].

Aside from the physical connections, there is also need, as mentioned before, to send the instructions as to what the IDE software should show as readings, through the Arduino programming language. Firstly, there is a need to calibrate the load cell, in order for it to measure the correct force in the desired work environment, due to the fact that there always external forces at play when the readings begin that need to be neutralized when it comes to readings, like the “tare” function on a weight scale. The required process to calibrate the load cell is, after the full work environment is built and it is in test conditions, to run the calibration code (found in Appendix F) without any weight on the cell, put a 50 g weight on the cell and check the monitor to see what values it prints, adjust the calibration factor by pressing the required keys on the keyboard, and once the printed value is 0.050±0.002-0.003 (kg), take a note of the calibration factor value and replace the one present in the code with the new one. After double-checking to see if the calibration factor is correct, the value was replaced in the code that will be used to read the load cell force values (found in Appendix G) with the correct one.

Finally, it is important to mention the method that will be used to actually record the measurement values of the test runs, since the Arduino IDE doesn’t record the values by itself. An extension, known as PLX-DAQ v.211 will be used to record the measured values and log them into the Microsoft Excel software. On the actual Microsoft Excel spreadsheet, a pop-up window with all the controls to begin, pause and end the test run is presented once the extension is installed and it is from there that user controls the data, which can then be exported to other excel spreadsheets and manipulated from there.

4.1.3 Test stand

When testing the power assessment of an ICE, a "dyno" (dynamometer-based) test stand is usually the most reliable choice. There are many different ways to acquire the data when it comes to dynamometer test stands, the two main ones are the inertia dynamometer and the steady-state dynamometer [21]. The first one works by accelerating an inertial mass using the engine until the data acquisition is complete and the full power and torque bands are logged [22]. The second category, on the other hand, uses a brake (also known as absorber) that applies a load to the engine, keeping it at a constant speed, while in WOT, and a load cell measures the torque transmitted to the brake [21]. Due to the lack of a functioning test stand, a reasonably reliable alternative was to build an improvised one that would be built to the same end, despite not being as accurate in terms of readings as an actual, factory designed one, due to the fact that this is a comparison study between the original cam in the Honda GX31, and the new one. In other words, even if the individual performance results are not equal to the expected values from the manufacturer's information, what really matters is the comparison between the two cams in terms of performance.

Having said this, it is important to understand the logic behind the improvised test bench and the differences between the built test stand and the ones mentioned before, starting with the basic principle behind this test stand, that lies on Newton's third law of motion, which states that any action will have an equal and opposite reaction. In this particular case, the crankshaft rotation creates a momentum, that is considered to be the action, and the propeller, despite rotating in the same direction as the crankshaft, will produce an equal and opposite momentum together with the engine block, the reaction [19]. With this in mind, the main objective of this test stand is to be able to quantify this reaction through the load cell mentioned in Section 4.1.2. In Figure 4.2 it is possible to visualize this process, considering that point A is the point at which the engine support platform is attached, through means of two ball joints and a metal plate, to the workbench, and point B is the point at which the resulting force is applied on the load cell, which is latched in place through means of four screws, two of them screwed from under the load cell and through the engine platform, and the other two screwed from the top of the other end of the load cell. Since torque is essentially a momentum, to obtain the torque values one has to multiply the resulting force, F (which is converted to Newton beforehand by multiplying the values by g=9,82 m/s^2) applied on the load cell, by the distance between point A and point B, which was named Z. From Figure 4.2 and the explanation given before, in order to retrieve the torque values from the applied force ones was solved:

$$T = F.Z\ [N.m] \tag{4.1}$$

for each one of the measurements of F. The value of Z was measured at 0.15 m and is constant throughout all of the test runs.

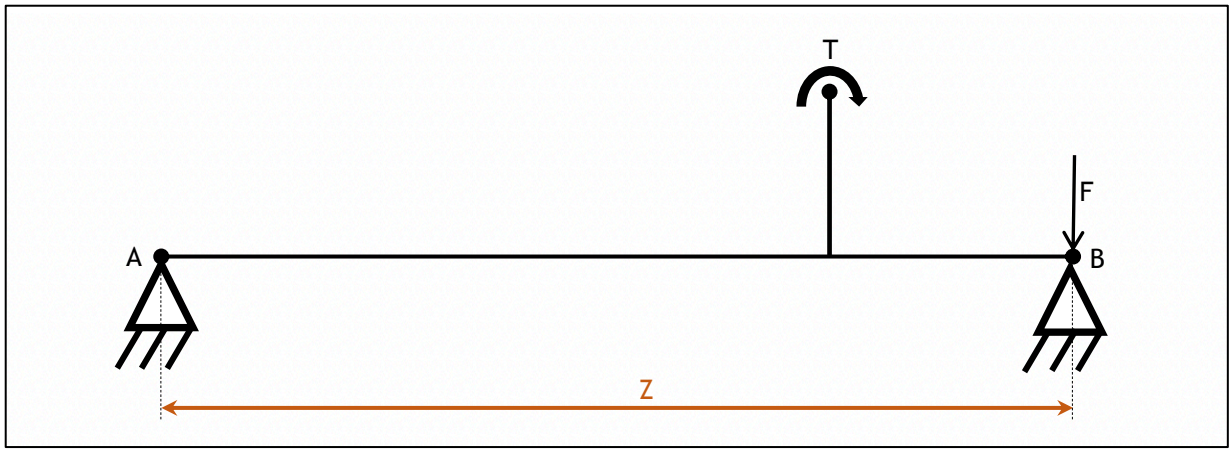

Figure 4.2 - Representative diagram of the test stand logic, based on [19].

Having said that, the process of building the test stand and how the different conditions affect the result outcomes will now be specified. First and foremost, the engine was coupled to a metal support that was manufactured in UBI during an earlier dissertation project, specifically for the Honda GX31, that consisted of two steel beams with square transverse sections, one with the side measuring 2 cm and another with the side measuring 4 cm. From the larger section beam, three sections were cut with resource to a metal-cutting saw and welded together in a "U" shape, with resource to a MIG/MAG welder to create a sturdy test stand base. Also, from the smaller section beam, a small segment was cut using a metal-cutting saw and welded on top of the "U" shaped section, in order to compensate for the engine's natural inclination and make it so it is always straight throughout the test runs. In order to reduce the friction, two ball joints were oiled and coupled to the engine support platform through means of two long screws and, through these two joints, a steel rod MIG/MAG welded to a small steel plate was placed with special care to make sure the platform could rotate, in order to allow the load cell to bend (see Fig. H.1 in Appendix H for a representation of the structure). Furthermore, the engine is locked in place to the support platform through means of four screws and the propeller was bolted onto the flywheel through means of a purpose fabricated, aluminium support.

Once the engine support platform is completed, the load cell has to be placed and, for this, a small wooden block was cut and perforated four times: two in order to fit the screws to attach the block to the workbench, parallel to the engine support platform, and two for the load cell screws that will lock it in place. The height of the wooden block is 4.5 cm, which makes it so the engine support platform is parallel to the workbench once it is latched to the load cell, as it is possible to visualize in Figure H.2 of Appendix H.

As it has been mentioned before, the Honda GX31 has a magneto ignition system which means that, due to the lack of an ECU, the engine speed will be measured with a Hall effect sensor to measure the magnetic spikes, connected to a digital automotive multimeter AT80B (see Fig. H.3 of Appendix H) and to a Li-Po, 3S battery. Due to the fact that the Hall effect sensor used needed to be powered

by a maximum voltage of 5 V and the available battery produced an output of 11.1 V, a battery eliminator circuit, or BEC, had to be connected in between the sensor and the battery in order to transform the original 11.1 V output into a 5 V output and, thus, not overloading and damaging the sensor.

One of the final components that need to be mentioned is the speed selector, or throttle body. Since the Honda GX31 has a carburettor admission system, the throttle butterfly valve is placed directly on top of the carburettor, with a support for one end of the throttle cable. A speed selector, similar to those present in lawn mowers, was bought, bolted onto the workbench directly behind the engine, and the throttle cable was adjusted in such a way that not only the butterfly valve's WOT and closed position coincided with both ends of the selector, but also that the cable tension, once the throttle was opened, was approximately zero, so that the load cell would not detect it as a measurable force. For this to happen, a small, metal, "L" shaped plate was designed to fit on the carburettor, as it is possible to see in Figure H.4 of Appendix H, and the full extent of the cable was mounted in the same direction as the engine platform support.

Finally, it is important to point out that extreme caution was employed at the time of the test runs, due to the fact that the propeller, once the engine is turned on, is rotating so fast that it is practically invisible to the naked eye and, even with its' tips painted red to try and improve the visualization of the propeller once in motion, a wooden box had to be manufactured in order to protect the operators (see Fig. H.5 of Appendix H), and once the engine was running, everything was operated from behind the engine. In the next section, a full description of the experimental procedure will be made.

4.2 Experimental procedure

When it came to the experimental procedure, it is important to point out that, in order to minimize the measurement errors, two people should always be doing the test runs together, due to the large number of tasks required for each test run. Furthermore, the operators should always be using protective equipment like gloves, soundproof earmuffs and masks, in order to prevent injuries and smoke inhalation.

First and foremost, since the engine was mostly disassembled, apart from the cylinder and head, all the missing parts were rigorously installed, according to the manufacturers' specifications. Furthermore, before starting the engine, it is important to check that all the bolts are correctly tightened in place, fill the engine with the manufacturer's recommended engine oil, to a maximum of 100 mL of SAE 10W-30, in the case of the Honda GX31 [23], check that both the intake and exhaust valve clearances are correct according to the manufacturers' information, inspect the spark plug for any visible damage and, by squeezing the carburettor's fuel pump a few times, remove the visible air bubbles inside the fuel lines.

After having made a complete engine check, the experimental procedure will be tightly followed, making sure that no steps are skipped and that everything is done with the maximum precision possible, in order to minimize the measurement errors that will be, inevitably, present due to the non-perfect conditions in which the test runs are made. The step-by-step process is as follows:

1. At the beginning of each test run, it was checked that the fuel deposit was filled with 86-octane or higher gasoline, as recommended by the manufacturer, and that the fuel filter was not clogged;
2. After weighing an empty, 250 mL of capacity, spray bottle (37,3 g in a digital weight scale that weighed a maximum of 300 g, for a more accurate reading) it was filled with same gasoline used for the engine;
3. Then, the digital multimeter is connected to the BEC through the terminals, using a "crocodile" type extension for each, it is turned on, using the selection knob and pointing towards the "1CYL" cycle reading, which is a function incorporated to the multimeter that reads the rotation of single-cylinder engines
4. The Li-Po battery is connected to the BEC through an appropriate terminal, in order for the Hall effect sensor to start working and the flywheel is, then, rotated by hand until the magnets cross the sensors' range, where an LED light flashes if the magnets are inside the range of the sensor;
5. Using the spray bottle, a graduated pipette coupled to a wooden, "L" shaped support, was filled to the 30 mL mark, taking care not to form any air bubbles;
6. Then, the spray bottle was weighed again to get an initial weight reading of the gasoline left in the bottle (by subtracting the empty bottle weight value to the measured one) and the value was registered on a Microsoft Excel spreadsheet that will be used to log all the values, both from the torque and from the fuel consumption;
7. Once the initial weight of the gasoline left in the spray bottle is registered, and the load cell calibration method mentioned in Section 4.1.2 is done, the PLX-DAQ v2.11 is initiated in the programs' Microsoft Excel spreadsheet and the data logging is paused, in order for the first read value of zero to already account for the initial conditions of the workbench, without the engine running;
8. After everything is ready, one of the operators turns on the engine, by coupling a purpose-built aluminium adapter with a silicone interior that is shaped like the propeller cone, to a power drill, which is then pressed against the propeller cone and turned anti-clockwise until the engine starts, applying the minimum possible force in order to avoid incidents;
9. While the power drill is rotating, in order to facilitate a cold start of the engine, the carburettor air intake is partially covered by the second operator, to enrich the mixture and the throttle valve is slightly opened so that the engine doesn't start completely in idle;
10. Once the engine starts, it is run for a few minutes at about 3200 rpm (since the idle speed is about 2700/2800 rpm at operating temperature), in order for it to gain the operating

temperature of about 70ºC and, to verify this, a digital thermometer equipped with a temperature probe sensor is connected and the probe is pressed against the engine body, until we get a stable temperature value;

11. As soon as the engine is at operating temperature, one of the operators is in charge of starting and pausing the data logging in the PLX-DAQ v2.11 and operating the stopwatch, while the second operator is in charge of changing the fuel flow from the fuel tank to the graduated pipette for the duration of the test run and back to the fuel tank again;
12. The test runs will have a duration of 20 seconds in which, in the first five seconds only the data logging system is acquiring the force values, once the stopwatch reaches the 5 second mark, the second operator changes the fuel flow from the fuel tank to the graduated pipette with the help of a "T" shaped tap (see Fig. H.6 of Appendix H) and as soon as the stopwatch reaches the 20 second mark (15 seconds later), the fuel flow is redirected again from the tank to the engine directly and the data logging is paused in the computer;
13. Afterwards, the first operator will copy the values of the first test run (about 80 force values per run, since the Arduino is programmed to read 4 values per second) to a separate Microsoft Excel spreadsheet, where all the force and fuel flow values will be stored and, in the meantime, the second operator will fill the pipette until it reaches the 30 mL mark again and weigh the spray bottle again, in order to get the initial and final weight values;
14. Then, the first operator registers the gasoline weight values, always subtracting the value of the empty spray bottle, in order to get the amount of fuel the engine consumed in that 15-second interval;
15. The process described in steps 11-14 is repeated 10 times for each engine speed, always making sure that the engine does not overheat and turning it off, through discharging the ignition coil by using a screwdriver to touch the armature metal pin and the exhaust manifold simultaneously, between engine speed changes to avoid any prolonged usage that may cause damage;
16. The test runs are made for a total of six different engine speeds, with 400 rpm intervals between each other, for a total of 60 test runs for each cam, starting with the original Honda GX31 cam and then switching to the new, aluminium cam.

In the next section, the experimental results will be presented and discussed, pointing out the difficulties and obstacles that surfaced during the experimental procedure and that may have affected the final results in one way or another.

4.3 Results and Discussion

Like it has been mentioned throughout this document, the main objective of the newly implemented cam is to widen the functioning power band of Honda GX31, making it a more stable, slower engine, without compromising too much in terms of performance, since the new cam has less valve lift than

the original one. After the procedure test runs mentioned in Section 4.2 were all done, the next step was to organize and format the data results in order to get a comparison between both cams.

After condensing all of the experimental results into two separate Microsoft Excel spreadsheets, one for the original cam and another one for the new cam, the first step when it came to getting the needed results was to get the average torque of each of the test runs, based on equation (4.1), ending up with a ten-point scatter for each of the engine speeds when it came to torque values.
The latter process was repeated to get the average power output of each test run, by using the following equation:

$$P = T.2\pi.\frac{N}{60}\ [W] \tag{4.2}$$

where T is the torque calculated from the load cell force measurements and equation (4.1) and N is test run engine speed, for each torque value and getting the average of each test run. Once the power output is solved, the next step is to get the SFC from the measured fuel flow, which can be gotten from:

$$\dot{f} = \frac{W_i - W_f}{15}\ [g/s] \tag{4.3}$$

where W_i is the fuel weight before each test run, W_f is the fuel weight at the end of each test run and 15 seconds is the measured interval for the fuel flow. Equation (4.3) is applied to every test run in order to get the fuel flow in each run and, afterwards, the results are used to get the SFC, which can be found through the following formula:

$$SFC = \frac{\dot{f}}{(P * 10^{-3})} * 3600\ [g/kWh] \tag{4.4}$$

in which $\dot{f}$ is the fuel flow from equation (4.3) and P is the average power output that results from applying equation (4.2) to each of the test runs. Resorting to the Microsoft Excel software, all the values are obtained at the same time once the formulas are formatted to the software's indentation and dragged to solve for all the cells.

After getting the average torque per test run, average power output per test run and SFC per test run of both cams, it is then possible to graphically compare the values between the two, keeping in mind that for the original cam the tested engine speeds were from 2700 rpm to 4700 rpm[16] with 400 rpm increments, and for the new cam from 2200 rpm to 4200 rpm, also with 400 rpm increments.

[16] The Honda GX31 has a wider power band to work with, but due to the workbench suffering from very high vibration at higher engine speeds than the last one tested, the load cell could not give accurate readings.

The following scatter plots depict this comparison, in which it is possible to observe different point scatters throughout the plotted values, which represent the average values of the ten test runs made for each engine speed, and an exponential trendline for each agglomerate of results (see Fig. 4.3).

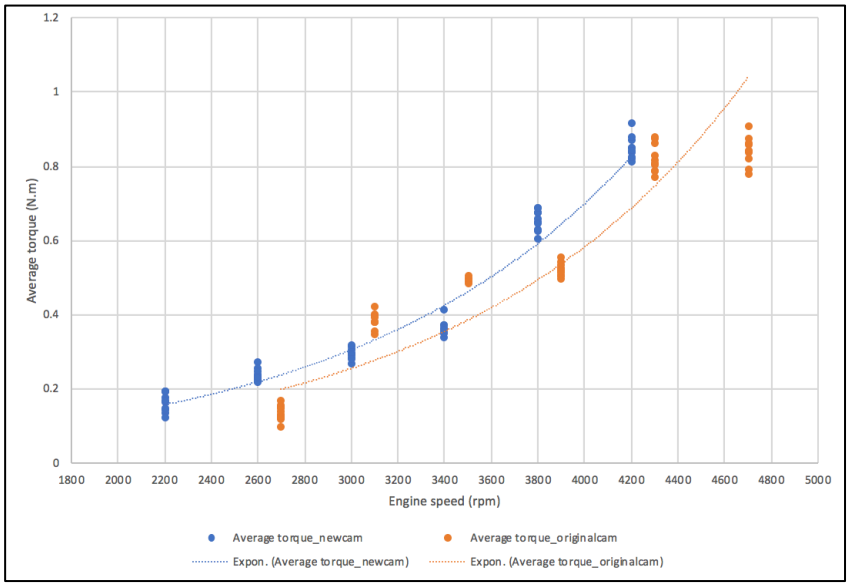

Figure 4.3 – Scatter point plot of the experimental results to show the graphical comparison between the average torque values of both configurations tested.

Firstly, it is important to mention that the average torque values obtained fall short of the maximum engine torque given by the manufacturer (1.64 N.m at 4500 rpm, according to the Honda GX31 user's manual), and this can be caused by a lot of different reasons, which will be explained later in this section. Nonetheless, and since this experiment was made in order to pursue a wider power band for the engine without compromising the actual performance values, the average torque results appear to be very positive, in the sense that, even though the results of the new cam configuration are not as high as the original cam at some engine speeds, they are very close throughout the entire interval, and even higher at some points. Also, the workable speed band of the engine has clearly shifted to lower engine speeds, without compromising nearly any performance values in terms of average torque, which is one more step towards fulfilling the main objective of this dissertation. It is also possible to observe that an exponential trendline was added to both point scatters in order to facilitate the visualization of the performance development, and their equations are as follows:

$$f(x) = 0{,}0215e^{0{,}0008x} \tag{4.5}$$

for the original cam configuration, with a coefficient of determination of $R^2 = 0{,}8201$, which is an acceptable value and means that the trendline function acceptably adapts to the data, and:

$$f'(x) = 0{,}0255e^{0{,}0008x} \tag{4.6}$$

for the new cam configuration, with a coefficient of determination of $R^2 = 0{,}9601$, which is nearly perfect and means that the trendline function adapts very well to the logged data.

Next up, in Fig. 4.4, is the average power output comparison between the two cams.

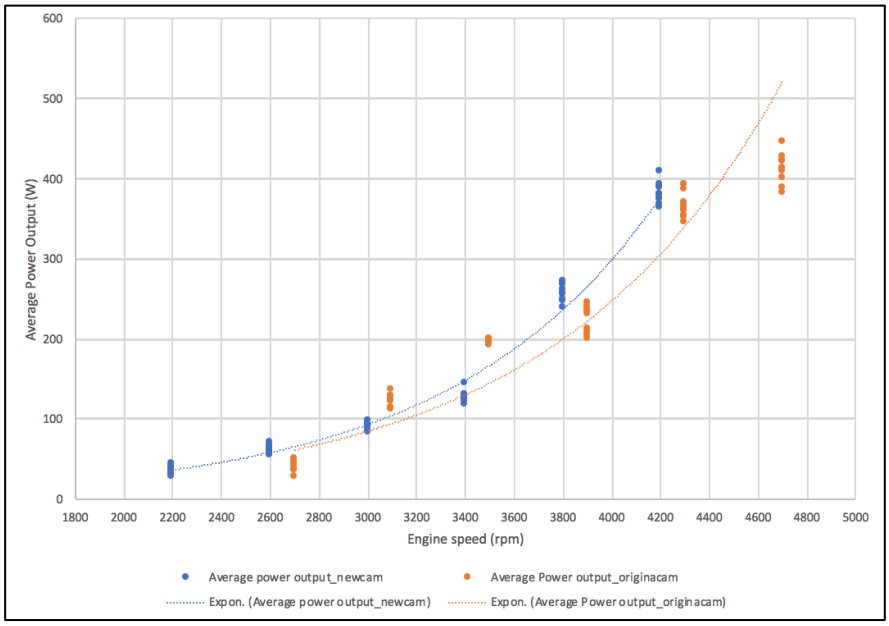

Figure 4.4 - Scatter point plot of the experimental results to show the graphical comparison between the average power output values of both configurations tested.

Likewise, the same variations are seen in this case, when it comes to absolute values in comparison with the expected ones (1100 W at 7000 rpm, according to the Honda GX31 user's manual), and as before, this can happen for a number of reasons which will be discussed further ahead. Despite this disparity, when comparing the performance behaviour of the two cams, it is, again, possible to conclude that the new cam configuration allows for more power on the low end of the power band and in some places on the higher end as well. Once more, the performance was favourably shifted to the lower engine speeds without sacrificing practically any performance. As before, exponential trendlines were added to better visualize the performance behaviour, and the equations are:

$$g(x) = 3{,}488e^{0{,}0011x} \tag{4.7}$$

for the original cam configuration, with a coefficient of determination of $R^2 = 0{,}8795$, which is a good value and means that the trendline function acceptably adapts to the data, and:

$$g'(x) = 2{,}85e^{0{,}0012x} \tag{4.8}$$

for the new cam configuration, with a coefficient of determination of $R^2 = 0{,}9817$, which is a practically perfect result, and means that the trendline function adapts very well to the logged data.

So far, the new cam configuration has proven better when it comes to the compromise between performance and eligible power band, which means that the dissertation objectives are close to being fulfilled.

Finally, for the SFC comparison between the two configurations is presented Fig. 4.5.

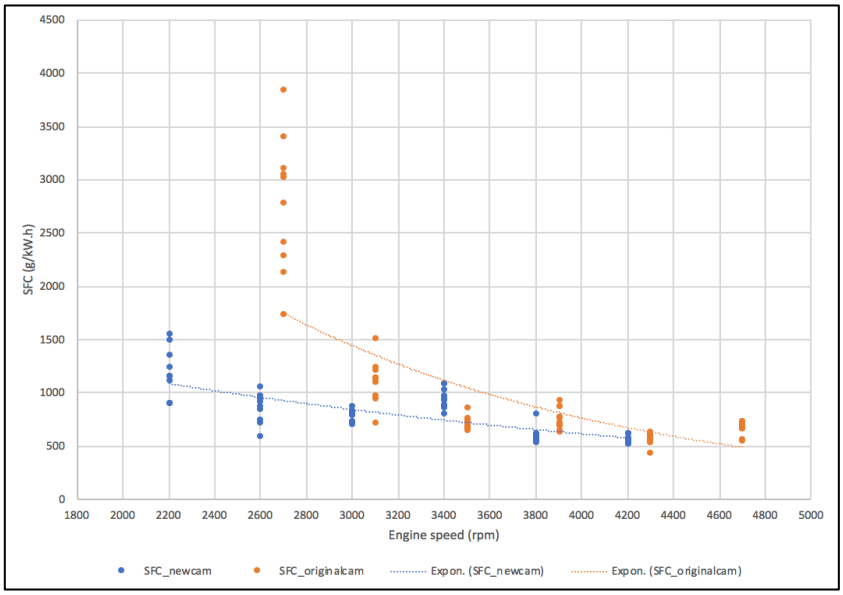

Figure 4.5 - Scatter point plot of the experimental results to show the graphical comparison between the SFC values of both configurations tested.

Once more, the absolute values of the SFC are far from the expected ones (350 g/kW.h, according to the Honda GX31 user's manual), despite the trendlines indicating that, at higher engine speeds, it could probably reach values close to the expected ones. Notwithstanding this, the pattern maintains itself, in the sense that once we compare the performance values between the two configurations, the SFC values with the new cam configuration are lower than with the original cam configuration, almost throughout the entire interval, which is a very positive result since we are talking about SFC. Like before, the visual shift of performance to the lower engine speeds anew proves that this is the path to follow in order for the engine to perform almost equally at lower power bands. The trendline equations, for this case, are:

$$h(x) = 9763{,}6e^{-6E-04x} \tag{4.9}$$

for the original cam configuration, with a coefficient of determination of $R^2 = 0{,}6471$, which is an average result, and means that the trendline function adapts to the logged data.

$$h'(x) = 2179{,}6e^{-3E-04x} \tag{4.10}$$

for the new cam configuration, with a coefficient of determination of $R^2 = 0{,}6044$, which is an average result, and means that the trendline function adapts to the logged data, despite not as well

as the original cam configuration, which means that the measurements were more consistent when the original cam configuration test runs were made.

Having said this, it is important to assess that the disparity in terms of actual numbers between the originally expected values and the experimental ones may come from different sources, which will now be discussed.

One example is the fact that the factory testing conditions of developed engine manufacturers, like Honda, are nearly perfect for the engine to perform at its' best, opposite to the testing conditions experienced throughout this experiment; another condition that may affect the performance values is that, like it has been mentioned in Section 4.1.3, there are different approaches when it comes to testing the performance of an ICE, and most engine manufacturers use the steady-state type, whereas in this experiment, an approximation of the inertia dynamometer was achieved, by varying the throttle position in between trials. Furthermore, even though the Honda GX31 is a very reliable engine, the one available for this project has had an extended usage, which means that some internal issues start to occur, namely the engines' ability to keep the expected values of cylinder compression. During the project, the cylinders' compression was tested using the appropriate engine-testing kit, in which the spark plug is removed and replaced by the threaded end of the compression gauge and afterwards, using the power drill and propeller adaptor, the engine is turned until a stable reading appears. The expected compression values were between 117 psi and 159 psi and the test revealed steady values of about 75 psi, which falls very short of what it should be and may contribute to the diminished performance.

Like it has been mentioned before, the Honda GX31 is a very high-revving engine in its' original configuration, which can lead to a very high level of vibration on the workbench. This could be seen throughout the test runs and was a big concern, due to the fact that every mechanical part has a limit to the vibration forces it can withstand, and some parts of the test stand, such as screws and welds, actually broke apart during some of the test runs due to the excessive vibration felt in the work environment, which meant that the test runs for that engine speed had to be restarted from the beginning, once the damage was repaired. Having to change parts will, obviously, diminish the consistency of the results, when it comes to precision, which is why, midway through the first trials, the test stand had to be moved to a different workbench due to the excessive vibration, and the test runs were restarted from scratch, to try and improve the precision of the experiment. It is also important to mention that this vibration phenomenon reduces the accuracy of the load cell readings, which is why the test runs for the original cam configuration were halted at 4700 rpm because above that, the load cell could not produce any accurate readings that could be used in terms of results.

When it came to the new cam configuration, the test runs were supposed to have continued through to higher engine speeds, due to the fact that this configuration offered much less vibration than the original cam configuration, but, halfway through the 4600 rpm test runs, one of the load cell locking

screws broke apart and damaged the thread inside the cell perforations. Even though this configuration offered a much smoother working environment in terms of vibration, it is crucial to point out the sheer number of tests the (already overused) engine had to be put through in order to get this many results, which eventually led to the excessive wear of some parts.

Another possible explanation for the difference between the obtained results and the expected ones is the fact that the manufacturer's torque curve is obtained in a constant WOT condition, whereas in the load-inducing propeller configuration, this condition was impossible to achieve. It could have been possible to achieve a similar testing point if the load induced by the propeller could be enough to have a constant WOT engine speed equal to the manufacturer's testing conditions, which did not happen.

Finally, it is important to point out how crucial it is to try and be precise when attempting to measure the valve lift, through the procedure mentioned in Section 3.1, for this will, afterwards, dictate the shape of the motion function and consequently, the cam profile design.

Chapter 5

Conclusions and future work

5.1 Conclusions

One of the first things to note is that the new cam configuration offered a much more stable, less vibratory, slower engine operation, which made it much easier to maintain the desired engine speed than with the original configuration, when it came to the test runs. This is much likely due to the fact that because both the duration and valve overlap were highly reduced, and therefore the engine is allowed to function with much more "room to manoeuvre". Moreover, and despite all the adversities faced throughout the experimental procedure, all the results were gathered with as much precision as possible and proven to be acceptably accurate when comparing both configurations. This proves that, even though more modern engines are available, like the Honda GX35, the present study can serve as the basis for any future projects that arouse, for the alteration of the cam-follower system is of crucial importance, in order to improve and adapt ICEs to the desired ends.

Apart from the actual manufacturing of the new cam, all the proposed objectives were accomplished, leading to the conclusion that if this study and design procedures are followed and applied to other, mechanically similar, engines, the usable power band of the engine can be lowered to more stable, slower engine speeds, without compromising the performance, which can allow the designer to over-dimension a propeller to fit to the engine and optimize its' performance for other purposes than the one it was initially designed for. Moreover, even though the structural analysis of the aluminium cam was not completed in this particular dissertation, it is of vital importance when attempting to design and actually manufacture any mechanical part, especially if it is part of the cam-follower system.

To sum up, it is possible to conclude that the present work might prove useful in the future when it comes to developing new technology and vehicles within and outside UBI and, in the next section, some suggestions for related future works are presented.

5.2 Future work

During the development of the present work, some topics were recognised as useful to implement in future works, when it comes to the present subjects, and they are as follows:

- Apply the present study to the Honda GX35 engine, which has a different cam-follower system and better performance output;
- Test the presented cam-follower system alterations with different intake configurations (like electronic fuel injection) to try to improve the volumetric efficiency that is diminished at high altitude;
- Implement larger propellers to the engine and study its' effect on the engine's performance output, with the presented cam-follower configuration;

Bibliography

[1] J. B. Heywood, *Internal Combustion Engine Fundamentals*, vol. 21. Cambridge, Massachusetts: McGraw-Hill Inc., 1988.

[2] Iluisolivan, "Tes blendspace." [Online]. Available: https://www.tes.com/lessons/dkfE1RfyuSJv5w/combustion-engines. [Accessed: 03-Apr-2018].

[3] S. Rajtiu, "The History of the Internal Combustion Engine," no. January, 2003.

[4] "Ideal Gas Laws and Heat Engines," 2015. [Online]. Available: https://www.andrews.edu/phys/wiki/PhysLab/doku.php?id=141s14l10. [Accessed: 26-Mar-2018].

[5] "4-Stroke Internal Combustion Engine (Otto)." [Online]. Available: http://www.learneasy.info/MDME/iTester/tests/10907_Engine_Performance/images/4-stroke.html.

[6] D. Arcoumanis, "Internal Combustion Engines," 2011. [Online]. Available: http://www.thermopedia.com/fr/content/880/. [Accessed: 10-Apr-2018].

[7] "Camshaft." [Online]. Available: http://energyeducation.ca/encyclopedia/Camshaft. [Accessed: 10-Apr-2018].

[8] "The engine - how the valves open and close." [Online]. Available: https://www.howacarworks.com/basics/the-engine-how-the-valves-open-and-close. [Accessed: 10-Apr-2018].

[9] J. E. Shigley and J. J. Uicker Jr, *Theory of Machines and Mechanisms*, Internatio. McGraw-Hill Inc., 1981.

[10] R. L. Norton, *Design of Machinery - An Introduction to the synthesis and analysis of mechanisms and machines*, Second. McGraw-Hill Inc., 1999.

[11] "History of VVT (Variable Valve Timing) technology," 2012. [Online]. Available: http://vtechauto.blogspot.com/2012/03/history-of-vvt-variable-valve-timing.html. [Accessed: 10-Apr-2018].

[12] J. Martins, *Motores de Combustão Interna*, Fourth. Publindústria, 2013.

[13] V. Reddy Chennu, "Honda VTEC System," 2015. [Online]. Available: https://me-mechanicalengineering.com/honda-vtec-system/. [Accessed: 11-Apr-2018].

[14] H. A. Rothbart, *Cam Design Handbook*. McGraw-Hill Inc., 2004.

[15] C. A. G. de Moura Branco, *Mecânica dos Materiais*. Porto: Fundação Calouste Gulbenkian, 1985.

[16] M. Ibrahim, "Elastic properties of three varieties of date Fruits during three different ripening stages," no. March, 2012.

[17] T. McQuade, "Honda GX-31 Specs." [Online]. Available: https://itstillruns.com/honda-gx31-specs-7602285.html. [Accessed: 24-May-2019].

[18] J. O'Clair, "Magneto Ignition System," 2011. [Online]. Available: https://www.hemmings.com/blog/article/magneto-ignition-systems/. [Accessed: 24-May-2019].

[19] J. Miguel Aguiar Caleira and F. Miguel Ribeiro Proença Brójo, "Controlo Eletrónico de um Motor Monocilíndrico," Universidade da Beira Interior, 2018.

[20] Arduino, "What is Arduino?," 2010. [Online]. Available: https://www.arduino.cc/en/Guide/Introduction. [Accessed: 10-Mar-2019].

[21] H. Cristiano Pereira da Silva Broeira, "Design of a Test Bench for Micro Combustion Engines," Instituto Superior Técnico, 2016.

[22] D. B. Johnson, N. M. Newberger, and I. C. Anselmo, "Vehicle Drivetrain and Method of Controlling Same.," EP2656041 B1, 2013.

[23] H. Engines, "Owner ' s Manual GX22-GX31," 2003. [Online]. Available: http://www.honda-engines-eu.com/documents/10912/23629/1389/81a6c28d-a0f2-4b16-8212-dec3e516586e. [Accessed: 24-May-2019].

[24] E. Specs, "Honda GX31." [Online]. Available: https://www.engine-specs.net/honda/gx31.html. [Accessed: 06-Jun-2019].

Appendixes

Appendix A

Table A.1 - Honda GX31 engine specifications [23], [24]

Honda GX31 Vertical Configuration Specifications		
Length	210	[mm]
Width	230	[mm]
Height	250	[mm]
Dry Weight	3.4	[kg]
Engine Type	Four-stroke, SI, single-cylinder	[-]
Valve arrangement	Overhead Valves	[-]
Intake Valve Clearance	0.12 ±0.02	[mm]
Exhaust Valve Clearance	0.15 ±0.02	[mm]
Displacement	31	[cm^3]
Bore x Stroke	39 x 26	[mm]
Max. Power Output	1100 (@ 7000 rpm)	[W]
Max. Torque	1,64 (@ 4500 rpm)	[N.m]
Idle Speed	3000±300	[rpm]
Max. rotation with no load	8500	[rpm]
SFC	340	[g/kW.h]
Compression Ratio	8.0:1	[-]
Cooling System	Forced air	[-]
Ignition System	Transistor magneto	[-]
Starting System	Recoil starter	[-]
Stopping System	Ignition primary circuit ground	[-]
Crankshaft rotation	Counter-clockwise	[-]
Fuel used	Unleaded gasoline (86-octane or higher)	[-]
Fuel tank capacity	0.65	[L]

Appendix B - Valve lift measurement equipment

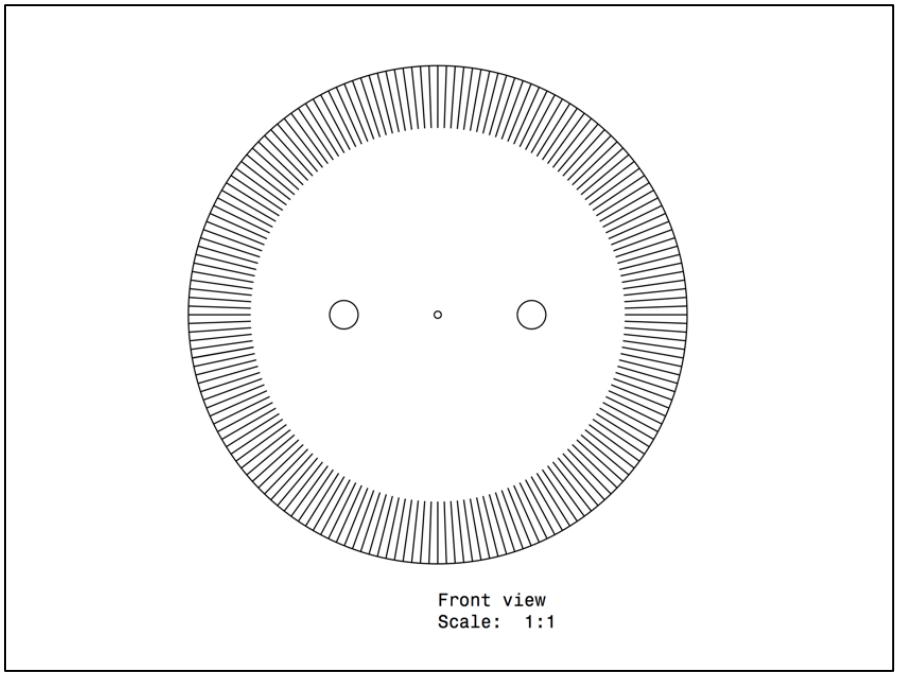

Figure B.1 - CATIAV5 draft of the graduated disk used to measure the valve lift.

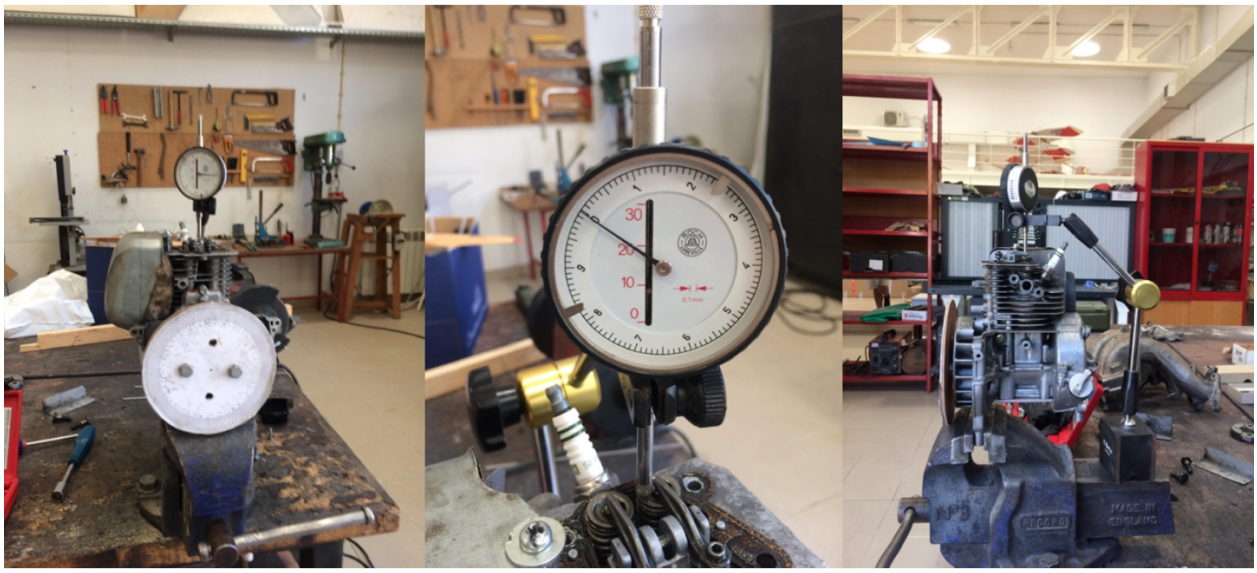

Figure B.2 - Graduated disk, analog dial indicator, articulated arm with a magnetic base and the Honda GX31 engine attached to the mechanical vice.

Appendix C

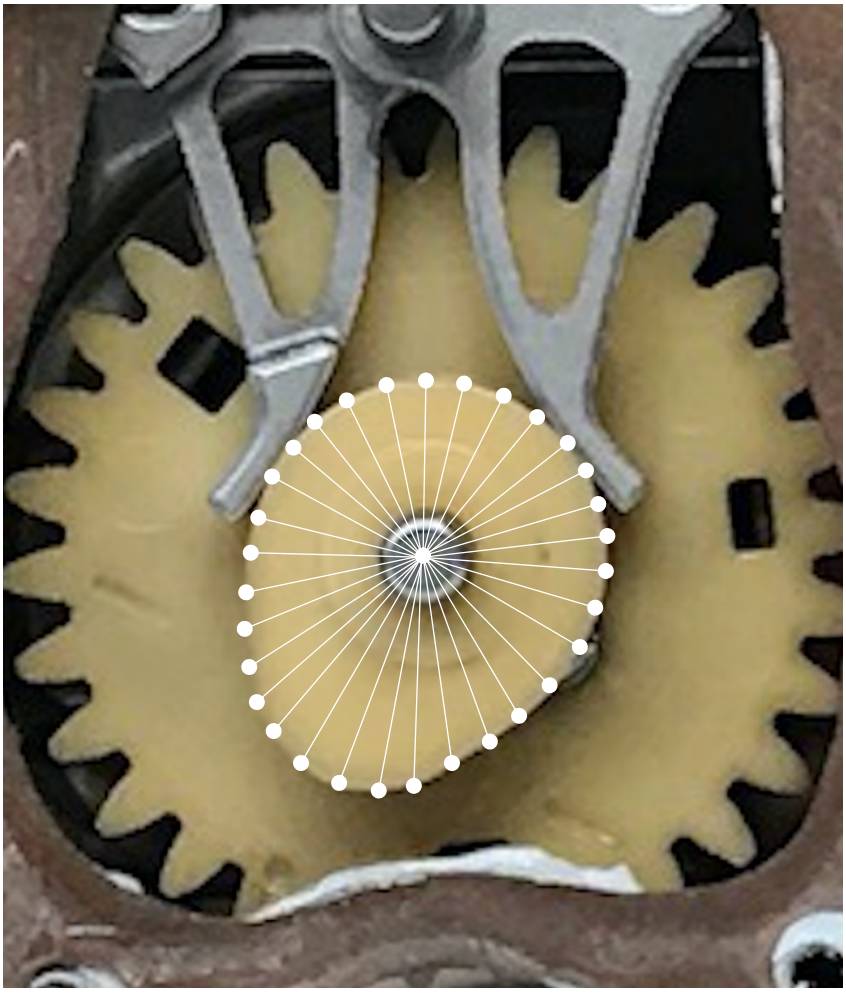

Figure C.1 - Detail of how R_{cam} varies throughout all the rotation positions.

Appendix D

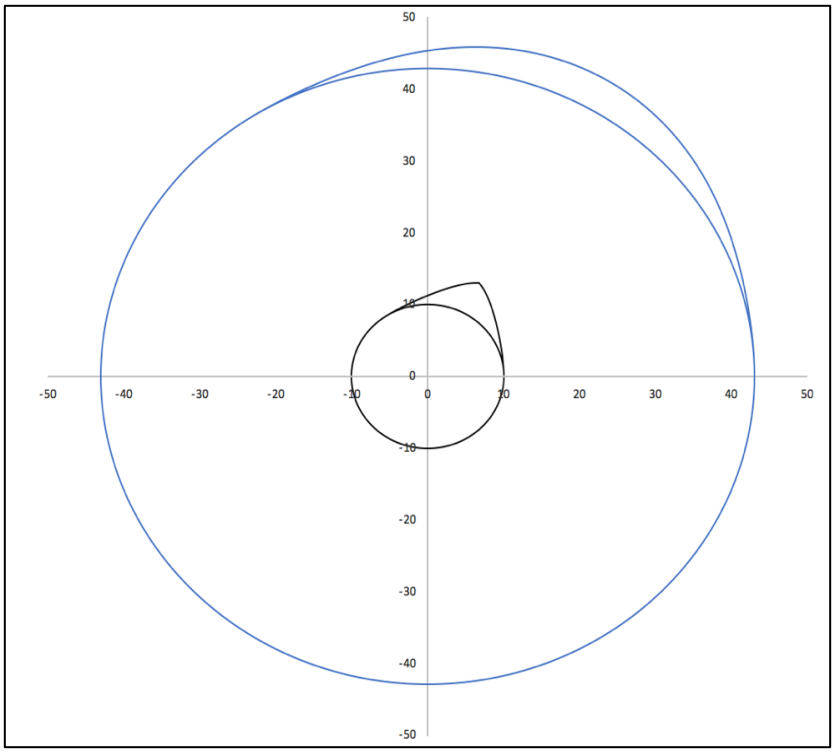

Figure D.1 - Detail of the unviable sharp-pointed cam profile resultant from the implemented model.

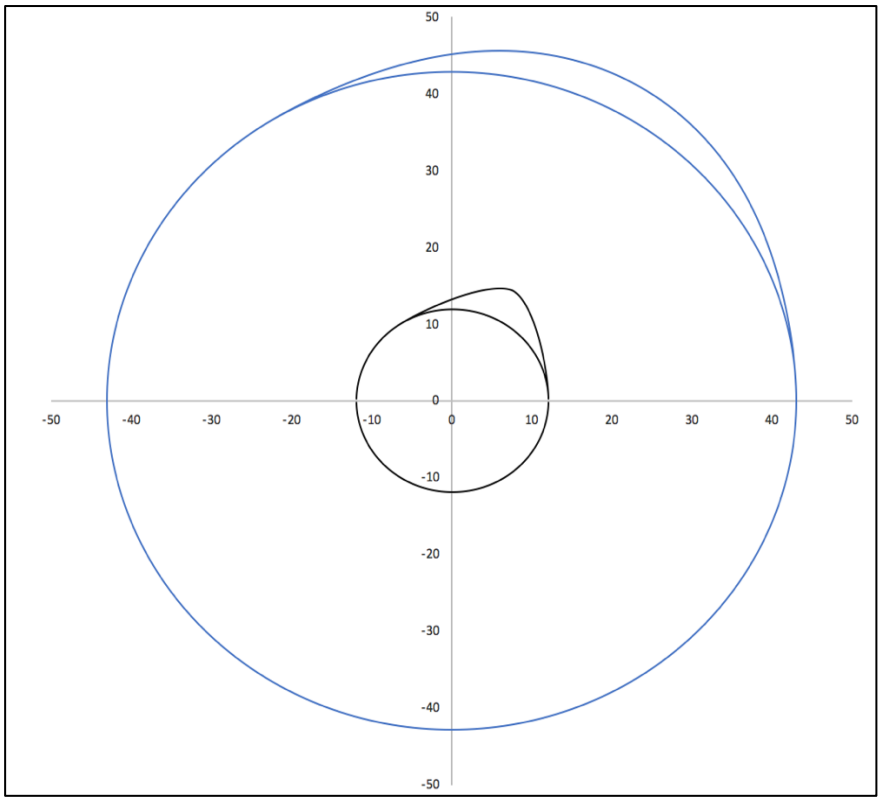

Figure D.2 - Detail of the smooth cam profile resultant from the implemented model that was supposed to have been manufactured.

Appendix E

Figure E.1 - Aluminium cam manufactured for the Honda GX31-powered Shell Eco-marathon vehicle.

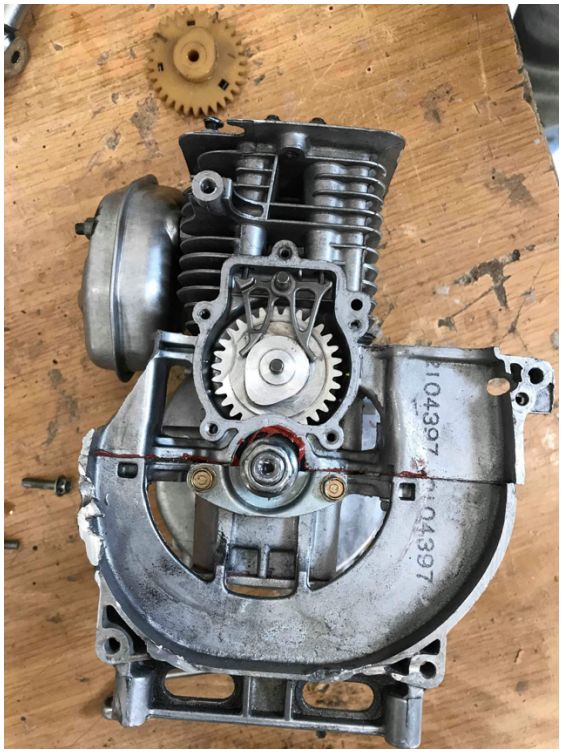

Figure E.2 - Aluminium cam installed in the Honda GX31 and, in the upper-right corner, the original Honda GX31 cam.

Appendix F – Arduino code used to calibrate the load cell

```
#include "HX711.h"

#define DOUT  3
#define CLK  2

HX711 scale(DOUT, CLK);

float calibration_factor = 243000 ;

//====================================================================================
//                    SETUP
//====================================================================================
void setup() {
  Serial.begin(9600);
  Serial.println("HX711 Calibration");
  Serial.println("Remove all weight from scale");
  Serial.println("After readings begin, place known weight on scale");
  Serial.println("Press a,s,d,f to increase calibration factor by 10,100,1000,10000 respectively");
  Serial.println("Press z,x,c,v to decrease calibration factor by 10,100,1000,10000 respectively");
  Serial.println("Press t for tare");
  scale.set_scale();
  scale.tare(); //Reset the scale to 0

  long zero_factor = scale.read_average(); //Get a baseline reading
  Serial.print("Zero factor: "); //This can be used to remove the need to tare the scale.
  Serial.println(867944);
}

//====================================================================================
//                    LOOP
//====================================================================================
void loop() {

  scale.set_scale(calibration_factor); //Adjust to this calibration factor

  Serial.print("Reading: ");
  Serial.print(scale.get_units(), 3);
```

```
  Serial.print(" kg");
  Serial.print(" calibration_factor: ");
  Serial.print(calibration_factor);
  Serial.println();

  if(Serial.available())
  {
    char temp = Serial.read();
    if(temp == '+' || temp == 'a')
      calibration_factor += 10;
    else if(temp == '-' || temp == 'z')
      calibration_factor -= 10;
    else if(temp == 's')
      calibration_factor += 100;
    else if(temp == 'x')
      calibration_factor -= 100;
    else if(temp == 'd')
      calibration_factor += 1000;
    else if(temp == 'c')
      calibration_factor -= 1000;
    else if(temp == 'f')
      calibration_factor += 10000;
    else if(temp == 'v')
      calibration_factor -= 10000;
    else if(temp == 't')
      scale.tare();  //Reset the scale to zero
  }
delay(1000);

}
//================================================================================
```

Appendix G – Arduino code used for the load cell readings

```
#include "HX711.h"

#define DOUT  3
#define CLK  2

HX711 scale(DOUT, CLK);

float calibration_factor = 243000; //Calibration Factor obtained from the calibration code

//============================================================================================
//                    SETUP
//============================================================================================

void setup() {
  Serial.begin(9600);
  Serial.println("Press T to tare");
  scale.set_scale(calibration_factor);
  scale.tare();            //Reset the scale to 0

 Serial.println("CLEARDATA");  //clears up any data left from previous projects
 Serial.println("LABEL,Time,Weight kg");
}

//============================================================================================
//                    LOOP
//============================================================================================

void loop() {
  Serial.print("DATA,TIME,");
  //Serial.print("Weight: ");
  Serial.println(scale.get_units(), 3);  //Up to 3 decimal points
  //Serial.println(" kg");

  //Serial.print("Time");
  //Serial.print("Weight");

  if (Serial.available())
  {
```

```
    char temp = Serial.read();
    if (temp == 't' || temp == 'T')
      scale.tare();  //Reset the scale to zero
  }
 delay(250);
}
//=============================================================================
```

Appendix H – Experimental components

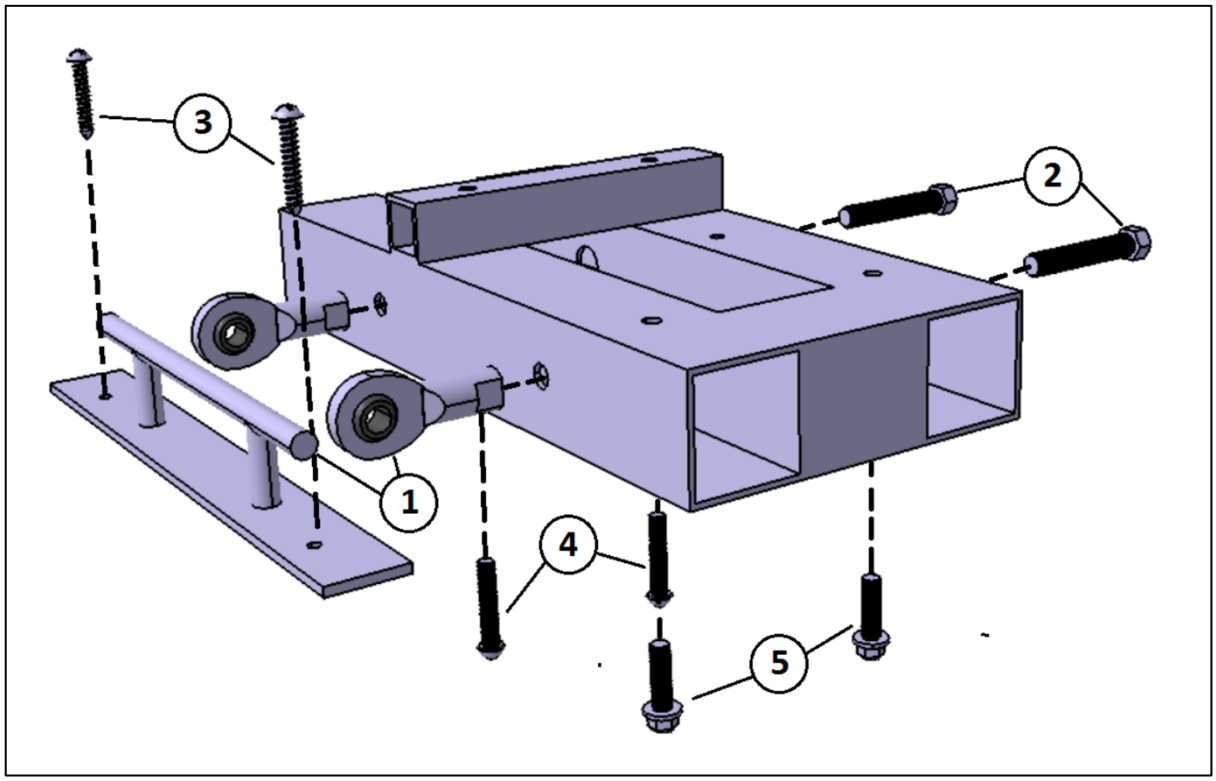

Figure H.1 - Representative CATIAV5 design of the engine support platform [19].

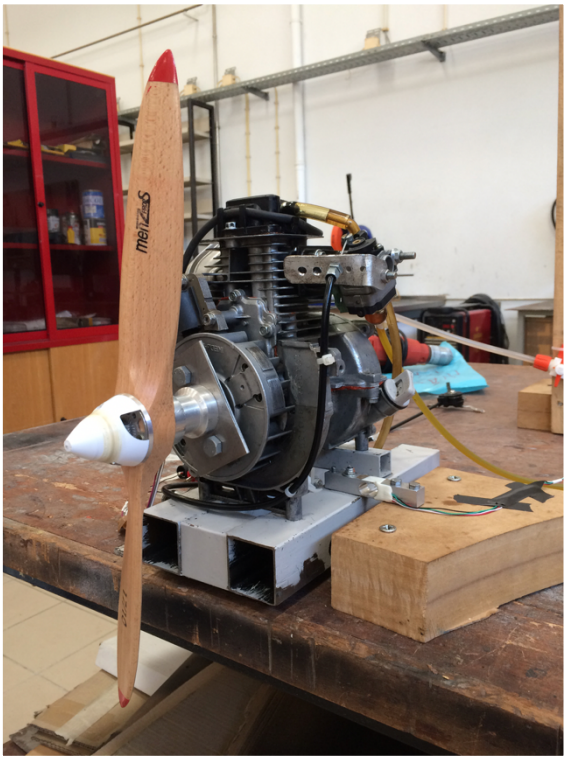

Figure H.2 - Photograph taken of the partial test stand environment, where it is possible to visualize the components mentioned in Section 4.1.3.

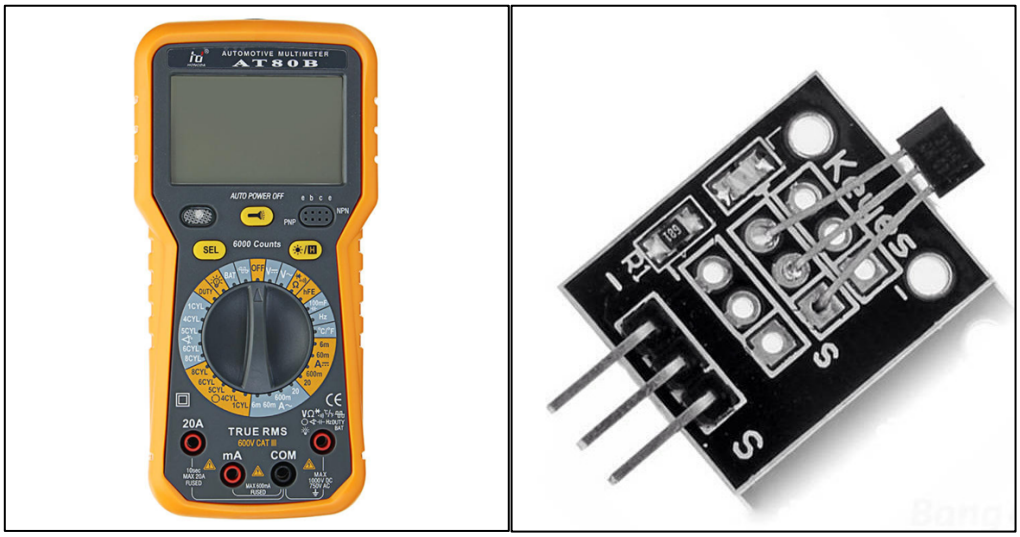

Figure H.3 - Automotive digital multimeter AT80B on the left and the Hall effect sensor on the right.

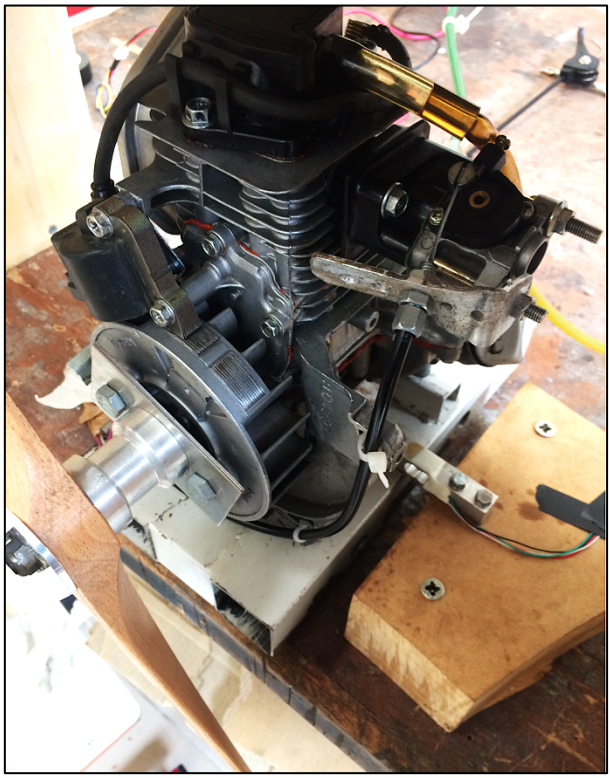

Figure H.4 - Detail of the throttle cable adapter coupled to the carburettor.

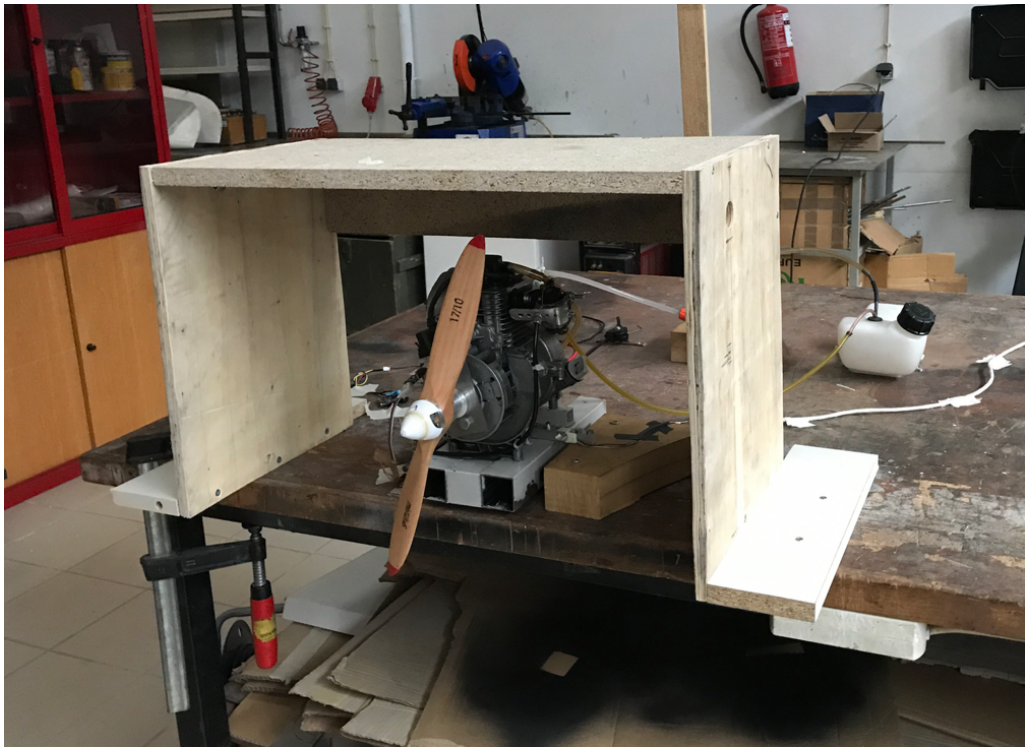

Figure H.5 - Partial experimental environment and wooden box detail.

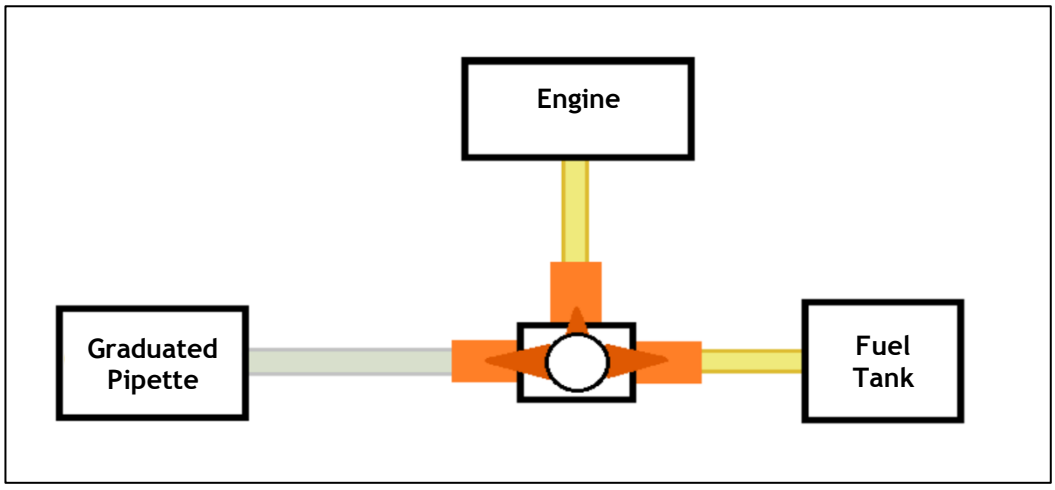

Figure H.6 - Adapted representation of the "T"-shaped tap used to control the fuel flow to the engine [19].

Figure H.7 - Detail of the Hall effect sensor in place, in order to read the magnetic pulses of the flywheel magnets during the test runs.

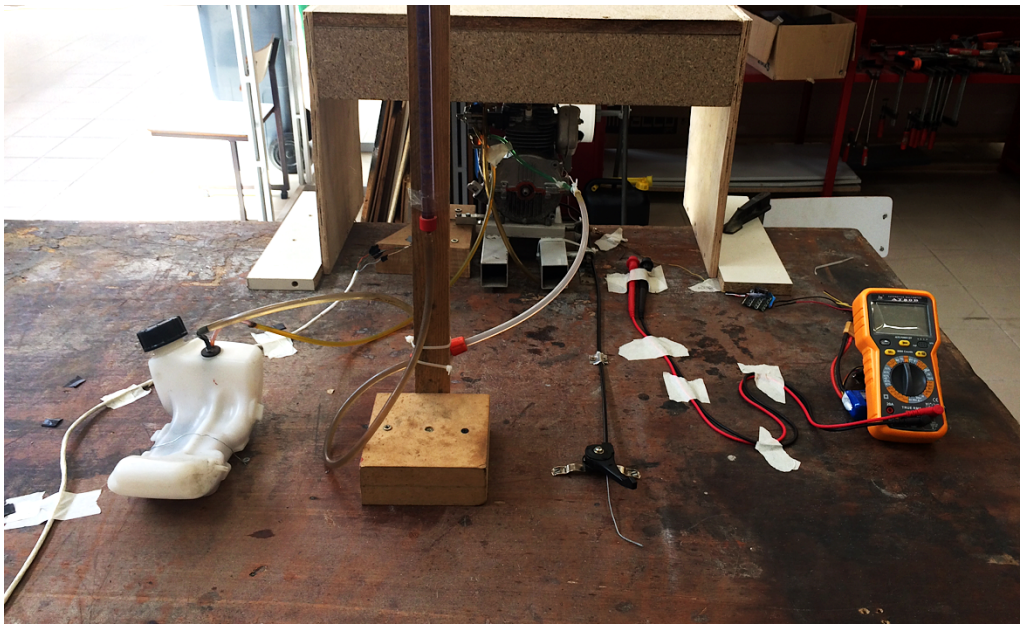

Figure H.8 - Full test stand configuration (with the exception of the breadboard containing the Arduino and HX711 connections).